16 Appendix B: Karst Investigation

Karst investigations and conceptual model of the bedrock aquifer at the proposed Nelson Quarry extensions

Stephen R.H. Worthington

Worthington Groundwater

April 25, 2020

16.1 Introduction

The existing Nelson Quarry and proposed extensions are located in dolostone rocks of the Goat Island and Gasport Formations. Flow in dolostone rocks is somewhat different from flow in sediments such as sand, and a common question is whether these rocks are karstified, and if so, what are the practical implications. This report described the investigations that were carried to answer these questions, and describes how water flows through the dolostone aquifer.

The Gasport Formation is named after Gasport, New York, which is 110 km east of Burlington. Goat Island is located between the Horseshoe Falls and American Falls, at Niagara Falls. The usage of these names such a long distance from the type localities is an indication of the lateral persistence of these rocks. Consequently, only minor variations in lithology are expected in the area of the site, and studies from elsewhere can inform the expected aquifer characteristics at the site. For instance, extensive measurements of the matrix of the rock have been made in the Smithville and Cambridge areas, showing that the mean porosity of the rock is about 7% and mean matrix hydraulic conductivity is about 10-7 m/s (Novakowski et al., 1999; Perrin et al., 2011). Pumping tests and numerical models of the site have shown that the total hydraulic conductivity of the aquifer is about 10-5 m/s to 10-4 m/s (see Azimuth and Earthfx reports). This shows that more than 99% of the flow in the aquifer is through the fracture network rather than through the matrix of the rock. This is a common situation in bedrock aquifers, which are referred to as dual-porosity aquifers.

The fractures in the rock were formed by physical processes such as tectonic stresses and unloading of the rock after the melting of the glacier that covered Ontario in the last ice age. Similar fracturing also occurs in shale, such as the Queenston Shale, which outcrops to the east of the Niagara Escarpment. However, the permeability of dolostone is on average four to five orders of magnitude greater than that of shale. The large difference is explained by the greater solubility and higher dissolution rate of dolomite, the main mineral in dolostone, compared to the minerals in shale such as quartz, illite and kaolinite (Worthington et al., 2016). Dissolution of the bedrock is focussed where the most flow is, which is along fractures. This results in a positive feedback loop, creating a network of solutionally-enlarged fractures through which most of the groundwater flows (Worthington and Ford, 2009). Bedrock aquifers where the permeability has been enhanced by dissolution are sometimes called karst aquifers, though there are a number of definitions for the term karst aquifer (Worthington et al., 2017). Where streams flow over dolostone bedrock, then there is the potential for substantial enlargement of underlying fractures, and on occasion these can be enlarged to become caves. However, percolation of rainfall into the bedrock favours the enlargement of the many interconnected fractures through which the water flows, producing a network of enlarged fractures (called channels, solutionally-enlarged fractures, or open fractures) that typically have apertures in the 0.1 mm - 10 mm range (Worthington and Ford, 2009).

The goal of the karst investigation in the study area is (a) to document the presence of surficial karst features that are relevant to aquifer hydrogeology such as sinking streams, springs, and discharges from quarry walls, (b) to carry out subsurface investigations to characterize the apertures and spacing of solutionally-enlarged fractures, and (c) to interpret the results to explain how water flows through the dolostone aquifer. These three tasks are described below in sections 2, 3, and 4, respectively.

16.2 Surficial karst features

2.1 Discharge from the walls of the existing quarry

An examination of quarry faces in winter can give a good indication of the nature of flow in a carbonate aquifer. Small discharges from such faces readily freeze and are visible as deposits of ice on the face. Major discharges may have enough flow of relatively warm groundwater that they only partially freeze, but the large flow of water is readily visible flowing down a quarry face. The quarry faces were visited on two occasions in cold winter conditions. Figure 1a shows the locations of photos taken and of sinks and springs, and Figure 1b shows the location of the wells referred to in this report. Figures 2 and 3 show typical accumulations of ice on quarry faces. In Figure 2, most of the discharge appears to be from several closely-spaced bedding planes close to the base of the face. Such flow is not unexpected because drawdown of the water table around the quarry by pumping from the quarry sumps should result in greater flow near the base of the quarry faces.

The higher parts of the face in Figure 2 as well as the section of face shown in Figure 3 have only sparse deposits of ice. These photos were taken on the eighth consecutive day of sub-zero temperatures, and the mean temperature in this period was -6.3 ^{o}C. Consequently, the ice that accumulated over this period only represents small discharges of groundwater, and represents flow from channels of a few millimetres or less in aperture. A feature of note is the much larger void shown in Figure 3 close to the base of the face. There was no flow of water from this feature, which consequently was an isolated void rather than part of the interconnected channel network.

The overall distribution of ice deposits on the face gives one indication that there is preferential flow in the aquifer along channels and that there are many such channels. The aperture of these channels is likely to be predominantly in the millimetre range.

2.2 Karst features on the extension lands and adjacent properties

The surface features of the South Extension lands were examined during the pumping test on February 10-13, 2006 and on several subsequent occasions. The first was a field trip to examine karst features on March 14, 2006 when Daryl Cowell, the peer review karst expert, was present. On that occasion the perimeter of the extension lands was visited and the East Arm of the West Branch of Mount Nemo Tributary was followed downstream to a sinkpoint (Figure 4) and a series of springs located in a dug pond that was 162 m to the south of the sinkpoints (Figure 5). The second was on March 22, 2006, when a tracer test was carried out at the sinking stream (Figure 6). The third occasion was March 23, 2006, when the extension lands were extensively searched for karst features. The Medad valley was traversed, from south of Lake Medad to the monitoring location SW02B (Figure 1). Several springs were located, and their electrical conductivity, temperature, and discharge were recorded (Table 1). In addition, the adjacent farm property between the extension lands and Guelph Line was also searched for karst features. Additional measurements were made on April 6, 2006 (Table 2).

A series of depressions in a wooded area along the south-east boundary of the property were visited on March 14, 2006. The deepest depression was about 10 m long, 6 m wide and 2 m deep. The consensus at that time was that the depressions represented small glacial kettle holes rather than karstic sinkholes. The visit on March 22, 2006 strengthened this opinion as two of the three largest depressions had standing water in them, covered by a layer of ice (Figure 7). This indicated that the permeability at the base of these depressions was extremely low. The largest depression had no standing water, however, indicating that the permeability at the base of this depression is somewhat higher than the other depressions. There were no channels entering this depression, no evidence of collapse, and the side slopes are gentle, so it is probably glacial rather karstic in origin. However, it is

possible that the focussing of recharge at one point has resulted in dissolution of the underlying bedrock.

In a low-lying wooded area in the south-west part of the extension lands there are a series of small springs. A number of small springs and seeps were noted in an area of 30 m by 30 m. The largest single spring had a discharge of less than 0.5 L/s. All the flows combine to form a creek that had a flow of 4 L/s at the property line, close to monitor OW3-32. The creek flows west from here to join the West Arm of the West Branch of Mount Nemo Tributary. The location of the springs in a shallow valley and the low discharge of these springs indicate they are likely to be depression discharges from the overburden, which has a depth of 1.02 m at OW3-32.

The surface features of the West Extension lands were examined on April 22, 2019. Only one potential karst feature was found, a closed depression about 25 m west of the southernmost of the artificial ponds on the golf course property. The landscape in this area has been heavily modified, so it is not possible to tell whether the depression is natural. Water was ponded in the base of the depression at the time of the visit, so it does not perform a karstic function at the moment, even if it is a natural depression.

With the exception of the sink to spring flow shown in Figures 4 and 5, there is a notable absence of surface karst features in or adjacent to the extension areas. This is in marked contrast to areas close to the Niagara Escarpment, where the overburden in thinner and karst features are common.

2.3 Characterizing the sink to spring connections

Two streams were found to sink into the ground in the study area, and it was assumed that these flow to nearby springs (Figure 1). This assumption was tested by tracer testing from the sink on the East Arm of the West Branch of Mount Nemo Tributary and by water level measurements on Willoughby Creek Tributary, as described below.

2.3.1 East Arm of the West Branch of Mount Nemo Tributary

To the south-east of the South Extension, the East Arm of the West Branch of Mount Nemo Tributary sinks into the ground at several sinkpoints (Figure 4). Several springs are located 162 m to the south (Figures 1 and 5). A fluorescent dye was injected into the sinking stream at the principal sinkpoint (Figure 6). Details of the test are given in Appendix A. The tracer travelled to the springs at a velocity of 1600 m/d, which is typical for conduit velocities in karst. There are several sinkpoints and springs, and flow between them is likely to be through several conduits in the shallow weathered bedrock. The sum of the calculated cross-sections of these conduits is 0.3 m^2.

2.3.2 Willoughby Creek Tributary

Willoughby Creek Tributary flows into a sinkhole downstream from the monitoring point on Colling Road at SW1 (Figure 1). A large spring 400 m to the west in the Cedar Spring valley (Spring K in Figure 1) was presumed to be the resurgence for this sinking stream. To confirm this, water levels were recorded at this spring at 15 minute intervals over a period of two weeks (Figure 8). Figure 9 shows greater detail of the water levels over the last three days of this period. Pumping from the quarry sump took place between 2 am and 5 am on these days. The spring water levels started to increase one hour after the start of pumping, and started to decrease one hour after the cessation of pumping. Part of this lag time is accounted for by flow along the surface creek so the lag time through the sink to spring connection is less than one hour (Figure 1). The short lag time indicates an efficient sink to spring conduit connection. Spring J has a similar electrical conductivity to the sinking stream, which suggests that the stream not only connects with Spring K but also with Spring J.

16.3 Tests using wells

Two types of well tests were used to characterize the aquifer. Pumping tests and tracer tests were both used to characterize the aquifer between wells, and are described in Section 3.1. Single-well tests included packer tests and flowmeter, video, televiewer, electrical conductivity and temperature logging. These are described in Section 3.2.

3.1 Tests between wells

3.1.1 Celerity values from pumping tests

Celerity refers to the speed of a pressure pulse. In aquifers, these are associated with decreases in pressure, such as during a pumping test, and increases in pressure, such as when the water table rises following rain or snowmelt. Celerities in unconfined aquifers can exceed 10 km per day, resulting in rapid response of springs and streams to rain and snowmelt events (Worthington, 2019).

There is a rapid decrease in water level in the pumping well when a pumping test starts, and the arrival time of the drop in pressure is routinely recorded in monitoring wells. Results from pumping tests at PW-1 in 2006 and BS-06 in 2019 give celerities of 3.9 km/d to 49 km/d (Table 3).

3.1.2 Tracer testing during the pumping test at PW-1

Tracer testing was carried out during the February 2006 pumping test to gain more knowledge on fracture apertures and on the connectivity of large-aperture fractures. A summary of tracer results are given in Table 4, and full details of the methodology and results are given in Appendix A.

Fluorescent dyes were introduced over three days into six bedrock monitors located from 14 m to 24 m from the pumping well. Traces from five of the six monitors used gave groundwater velocities of 72 - 160 metres per day, indicating efficient connection with the pumping well through channels. It is likely that many of these channels have diameters in the range 0.1-1 mm, a smaller number are in the range 1-10 mm, and relatively few have diameters > 1cm. The tracer from the sixth monitor was not recovered when the pumping test was terminated 24.3 hours after injection, and this showed that there was no efficient channel connection between this monitor and the pumping well.

3.2 Single well tests

3.2.1 Packer tests

Packer tests made a series of measurements of transmissivity in a well. Packer testing was carried out by Golder Associates in 2003 and by Azimuth in 2019, and results are found in the respective reports. Results presented here are for calculations of fracture characteristics from the packer test results. The calculated mean hydraulic conductivity from the packer testing is 6.15×10^{-5} m/s, with a standard deviation of log hydraulic conductivity of 0.79 (Table 5). This table also shows calculated fracture apertures for the most transmissive interval, assuming that the transmissivity in each well is associated with a single fracture.

The hydraulic conductivity in each well was measured by packer testing, and this enables the aperture of the flowing fractures to be estimated from the cubic law

$K = \rho g N b^3 / 12\mu$

where K is the hydraulic conductivity, ρ is the density of water, g is gravitational acceleration, N is fractures per unit distance, b is fracture aperture, and μ is dynamic viscosity. The calculated maximum fracture apertures for each well are given in Table 5.

The testing in 2019 used a much smaller test interval (~1 m) than the 2003 testing (~3m). The smaller interval allows more accurate determination of fracture porosity values, so only the 2019 data were used to determine fracture porosity. The individual fracture apertures for each tested interval in each well were summed to give the total fracture apertures for each well. These were then divided by the sum of the tested intervals to give the fracture porosity, which ranged from 0.00013 to 0.00059 (Table 6).

3.2.2 Video, televiewer, and flowmeter logging

Video and televiewer logs do not directly produce quantitative data, but they are nevertheless invaluable for developing conceptual models of bedrock aquifers. These visual logs are ideally coupled with measurements of flow from flowmeter logs or of transmissivity from packer tests. The combination shows whether flow in a bedrock aquifer is mostly seeping slowly through the pores of the rock, or whether there is more rapid flow through fractures. If the latter is true, then the shape of the fractures can show whether their apertures are due solely to physical stresses, or whether weathering has dissolve the rock to produce elliptical channels. Select video, televiewer, and flowmeter logs are shown in Appendix B. The full logs are found in the respective Golder and Azimuth reports.

Flow in the dolostone aquifer is principally through fractures, and the fractions of total flow through the most productive fractures can be calculated from flowmeter or packer test data. Results are shown in Table 7, and these results are compared to data from the literature in Figure 10.

3.2.3 Electrical conductivity and temperature logging

Profiling of electrical conductivity and of temperature at monitoring wells during pumping tests can help show the nature of preferential flow in bedrock aquifers, and how water quality can change over time (Worthington and Smart, 2017). Profiling was carried out at Well BS-07 before, during, and after the pumping test at BS-06 in October 2019. Profiling was also carried out in the pumping well before and after the pumping test. Further details and the results are found in Appendix C.

16.4 Conceptual model of the dolostone aquifer

4.1 Large conduits

Large conduits were identified at two locations in the Mount Nemo plateau (Section 2.3). Tracer testing of the 162 m long sink to spring connection on the East Arm of the West Branch of Mount Nemo Tributary gave an estimated conduit cross-section of 0.3 m^2. This is probably divided between several conduits. The conduit along Willoughby Creek Tributary drains a larger area and thus may be larger in size if it is a single conduit. The depth of these conduits is unknown. However, Worthington (2001) showed that depth of conduit flow below the water table is a function of both stratal dip and flow path length. The shallow stratal dip (0.4^o at the extension lands) and the short flow paths between sink and spring give predicted conduit depths of less than 1 m below the water table. While such a calculation is not exact, it does indicate that these major conduits are in the upper part of the bedrock.

Further large conduits (with diameters greater than 10 cm) are also likely to occur upgradient of and close to the larger springs that are found at the perimeter of the Mount Nemo plateau. It is possible that large conduits were formed between sinking streams and springs before the last glaciation. It is

most likely that such ancient conduits linking sinks to springs would also have formed in the uppermost bedrock and consequently would have been eroded away during the subsequent glaciation.

4.2 Open fractures

The observations of discharge at the quarry faces (Figures 2 and 3) show that there are many open fractures in the aquifer. The occurrence of many small springs along the Medad Valley (Table 1 and Figure 1) gives an indication of how dissolution and self-organization of flow in the aquifer results in flow to many smaller springs rather than one or two large springs.

The testing between wells (Section 3.1) demonstrates the connectivity of open fractures between wells. Pressure pulses from pumping tests or recharge events propagate through the network of open fractures, and result in the high celerity values of 3.9 km/d to 49 km/d (Table 3). Calculations from tracer testing between wells gives calculated apertures of less than 1 mm (Table 4).

The testing within wells (Section 3.2) gave complementary data of fracture characteristics. Packer testing allows the calculation of maximum fracture apertures (0.17 mm to 1.59 mm - Table 5) and fracture porosity (0.00019 - 0.00059 - Table 6). This porosity largely represents the porosity of bedding-plane fractures. These are much more likely to be intersected by wells than joints, which are almost all close to vertical. The addition of joint porosity would increase fracture porosity somewhat, perhaps to about 0.001. The fracture aperture and fracture porosity calculations in Tables 4, 5, and 6 are all based upon the assumption that fracture flow is through smooth, straight, constant aperture fractures. However, televiewer logs show that fracture enlargement along bedding planes is irregular. This is because dissolution enlarges fractures, with the most dissolution occurring where there is the most flow. This results in a positive feedback loop where parts of the bedding plane are enlarged to form elliptical channels that may have apertures >1 cm, while much of the bedding plane remains minimally enlarged. This is illustrated well in the televiewer images at depths of 1.85 m, 8.09 - 8.13 m and 18.79 - 18.84 m in BH06-1 (Appendix B, pages 31-33) . Occasionally, a well may intercept a joint, and flow from a joint in BS-05 is shown by the flowmeter log, with the televiewer logs showing that the joint is intercepted from a depth of 11.55 m to 12.10 m (Appendix B, page 36). The preferential enlargement of fractures by dissolution results in maximum apertures that are always somewhat larger than are indicated by calculations such as those in Tables 4, 5, and 6.

Packer testing, televiewer, flowmeter and electrical conductivity logs all help show the spacing of the major flowing fractures in a well. Typically half the flow in a bedrock well comes from the most productive fracture, and 20% and 10% come from the second and third most productive fractures, respectively. Measurements show this to be the case in the dolostone aquifer in the study area (Table 7), and it is also true globally, not just in carbonate aquifers but also in other bedrock lithologies (Figure 10).

The data presented above shows that fracture porosity is very low (~0.001) and is much less than the porosity of the matrix (~0.07). Consequently, almost all the storage is in the matrix. Conversely, the hydraulic conductivity of the matrix (~10^{-7} m/s) is very low, and is only a very small fraction of the bulk hydraulic conductivity of the aquifer (~10^{-5} to 10^{-4} m/s). Consequently, almost all the flow is through the fracture network. This combination of properties makes the aquifer a dual-porosity aquifer, like many bedrock aquifers.

4.3 Does the dolostone behave as a karst aquifer?

A common question is whether carbonate aquifers are karst aquifers. This question is considered to be an important one by some hydrogeologists, who divide carbonate aquifers into karstic aquifers and non-karstic aquifers, and who consider that numerical of flow and transport in the former is less predictable than in the latter. The problem in answering this question is that there are several

conflicting definitions of what constitutes a karst aquifer. Worthington et al. (2017) discuss the five major definitions. The aquifer is karstic according to two definitions, having solutionally-enlarged fractures and a hydraulic conductivity >10^{-6} m/s. The aquifer is not karstic according to one definition because it has no caves, and is sparsely karstic according to two definitions, having little turbulent flow and few karst landforms. However, classifying the aquifer as karstic or non-karstic is not important; instead, the important issue in the context of developing a quarry is to understand aquifer behaviour.

A useful way to consider aquifer predictability is to assess the variability between wells by calculating the standard deviation of the logarithm of either transmissivity (SD log T) or hydraulic conductivity (SD log K). A karst aquifer in England which has many caves has SD log T of 1.31, while three other English limestones which are generally considered as not karstic and have very few caves have SD log T values of 0.74, 0.76, and 1.02, respectively (Worthington and Ford, 2009). The SD log K value in the study area for the packer test data is 0.79 (Table 5), suggesting that the aquifer is towards the more predictable end of the spectrum of carbonate aquifers.

4.4 Practical consequences of the aquifer structure

The low value of SD log K reflects the common occurrence of solutionally-enlarged fractures in wells, which shows that the network has a dense network of these fractures. This means that treating the aquifer as an equivalent porous medium can give reliable results for steady-state modelling of flow. However, transient modelling of flow and modelling of transport are somewhat more complicated because of the dominance of fracture flow over the short-term such term, and the addition of drainage from and recharge to the matrix over the long term such as seasonally (Worthington et al., 2019). If this transience is properly accounted for, then there is no reason why numerical models should not give good results for transport.

16.5 References

Golder Associates, 2004, Hydrogeological and water resources assessment of the proposed Nelson Quarry Co. Extension.

Novakowski, N., P. Lapcevic, G. Bickerton, J. Voralek, L. Zanini and C. Talbot, 1999, The development of a conceptual model for contaminant transport in the dolostone underlying Smithville, Ontario. National Water Research Institute, Burlingon, Ontario, 98 p.

Perrin, J., Parker, B.L, Cherry, J.A., 2011. Assessing the flow regime in a contaminated fractured and karstic dolostone aquifer supplying municipal water. Journal of Hydrology, 400, 396-410.

Worthington, S.R.H., 2001. Depth of conduit flow in unconfined carbonate aquifers, Geology, 29, 335-338.

Worthington, S.R.H., 2019. How preferential flow delivers pre-event groundwater rapidly to streams. Hydrological Processes, 33, 2373-2380.

Worthington, S.R.H., Ford, D.C., and Beddows, P.A., 2000b. Porosity and permeability enhancement in unconfined carbonate aquifers as a result of solution, in Speleogenesis: Evolution of karst aquifers, Eds. A. Klimchouk, D.C. Ford, A.N. Palmer and W. Dreybrodt, National Speleological Society, Huntsville, p. 463-472.

Worthington, S.R.H., and D.C. Ford, 2009, Self-organized permeability in carbonate aquifers. Ground Water, 47, no. 3, 326-336.

Worthington, S.R.H. and Smart, C.C., 2017. Transient bacterial contamination of the dual-porosity aquifer at Walkerton, Ontario, Canada. Hydrogeology Journal, 25(4), pp.1003-1016.

Worthington, S.R.H., Davies, G.J., and Alexander, Jr., E.C., 2016. Enhancement of bedrock permeability by weathering. Earth-Science Reviews, 160, 188-202.

Worthington, S.R.H, P-Y. Jeannin, E.C. Alexander, Jr., G. J. Davies, and G.M. Schindel, 2017. Contrasting definitions for the term ‘karst aquifer’. Hydrogeology Journal, 25, 1237-1240.

Worthington, S.R.H. Foley, A.E. and Soley, R.W.N., 2019. Transient characteristics of effective porosity and specific yield in bedrock aquifers. Journal of Hydrology, 578, 124129.

16.6 Tables and Figures

Table 1 Location and details of springs and creek flows measured on March 23, 2006

Grid easting (m)	Grid northing (m)	Electrical conductivity (µS/cm)	Temp. °C	Discharge (L/s)	Notes
590413	4802022	1095	7.7	2	by tank, <50 m from road
590416	4802034	793	7.9	1	
590343	4802077	758	8.3	-	
		853	8.7	5	5 m to north, Spring A
590343	4802081	836	8.4	1	at foot of slope
		799	8.6	1	2 m to north
590236	4802270	842	6.9	5.5	Circular spring in flood plain, flows into L. Medad, Spring B
590230	4802317	803	7.3	0.5	5 m from base of slope, flows into L. Medad
590218	4802352	769	7.3	0.3	below old track, flows into L. Medad
590140	4802486	616	7.3	0.3	at foot of slope, flows into L. Medad
590143	4802506	794	7.1	1.5	behind pump house, flows into L. Medad
590091	4802514	845	7.8	27	north of pump house, flows into L. Medad, Spring C
589963	4802693	881	7.1	1.5	
589993	4802740	809	6.8	0.5	
589915	4802708	779	7.4	3	Spring D
		776	6.7	2	10 m further north, headwaters of L. Medad
589890	4802789	843	6.8	1	in oil pipeline right of way, headwaters of creek flowing north
589880	4802813	722	7.3	3	Spring E
		833	7.5	3	15 m further north, Spring F
589725	4803103	747	5.5	1.5	
589696	4803176	773	5.9	2	
					Dense cedar - end measurement of springs < 3 L/s
589603	4803460	619	7.5	5	Spring G
589259	4803986	989	7.8	3	Spring H
588889	4804485	762	1.2	35	Creek in middle of valley at Second Sideroad right of way
				206	Willoughby Creek at Britannia Road (SW2)

Note: grid locations are with respect to the NAD27 grid

Table 2 Location and details of springs and creek flows measured on April 10, 2006

Electrical conductivity (µS/cm)	Temp. °C	Discharge (L/s)	Notes
1231	8.9	5	discharge from quarry at Colling Road (from small pipe)
1196	12.6	19	Willoughby Creek Tributary at Colling Road (SW1)
1219	6.4	5	Spring J (east of road)
1127	8.9	32	Spring K, at outlet from lake below waterwheel
882	10.1	140	Willoughby Creek at Britannia Road (SW2)

Table 3. Celerity values from pumping tests

Pumping well	Monitoring well	Distance from pumping well (m)	Celerity (m/d)
PW-1	MW03-04	13	3900
	OW03-22	17	8160
	OW03-23	38	16,600
	OW03-24	63	19,300
	OW03-25	57	17,500
BS-06	BS-03	17	49,000
	BS-07	37	15,200

Table 4. Groundwater velcities and fractures apertures from tracer tests to PW-1

Well	Tracer velocity (m/day)	Distance to PW-1 (m)	Channel diameter (mm)
MW03-04A	160	13.7	0.095
MW03-04B	<14	13.7	<0.046
MW03-04B	<14	13.7	<0.028
OW03-22A	72	16.1	0.066
OW03-22B	110	16.1	0.27
OW03-22B	110	16.1	0.15
OW03-27A	120	23.7	0.091
OW03-27A	120	23.7	0.093
OW03-27B	130	23.7	0.19
OW03-27B	130	23.7	0.095
OW03-27B	130	23.7	0.19
OW03-27B	130	23.7	0.096

Table 5. Fracture transmissivities and apertures from packer tests

Well	Hydraulic conductivity (mean- m/s)	Hydraulic conductivity (highest value - m/s)	Fracture aperture (assuming single fracture - mm)
BS-01	3.70E-4	2.50E-3	1.59
BS-02	2.03E-4	1.94E-3	1.46
BS-03	9.19E-6	7.13E-5	0.49
BS-04	1.97E-6	7.17E-6	0.23
BS-05	1.30E-4	2.3E-3	1.54
MW03-01	7.58E-6	1.1E-5	0.26
MW03-02	8.20E-6	1.6E-5	0.29
MW03-03	1.59E-6	3.3E-6	0.17
MW03-04	4.12E-6	1.0E-5	0.25
MW03-07	2.94E-5	1.5E-4	0.62
MW03-08	2.48E-5	5.4E-5	0.44
MW03-09	1.47E-6	5.3E-6	0.20
MW03-10	7.62E-6	2.9E-5	0.36
Mean	**6.15E-5**		
Standard deviation of log K	**0.79**		

Table 6. Fracture porosity from packer tests

Well	Sum of apertures (mm)	Sum of tested intervals (m)	Fracture porosity
BS-01	8.79	14.99	0.00059
BS-02	12.27	21.21	0.00058
BS-03	3.18	16.59	0.00019
BS-04	2.62	20.60	0.00013
BS-05	8.14	21.50	0.00038
Mean			**0.00037**

Table 7. Percentage of the total flows in each well that come from the most productive fractures

Well	Test method	Interval with highest flow or transmissivity (%)	Interval with second highest flow or transmissivity (%)	Interval with third highest flow or transmissivity (%)
OW3-30	Flowmeter	43.2	35.1	13.5
OW3-31	Flowmeter	51.5	24.2	13.3
BS-05	Flowmeter	67.9	20.5	11.4
BS-01	Packer	42.3	25.4	18.6
BS-02	Packer	36.7	17.8	9.6
BS-03	Packer	40.5	22.6	13.5
BS-04	Packer	17.9	13.9	10.1
BS-05	Packer	83.9	2.2	2.2
Mean		**48.0**	**20.2**	**11.5**

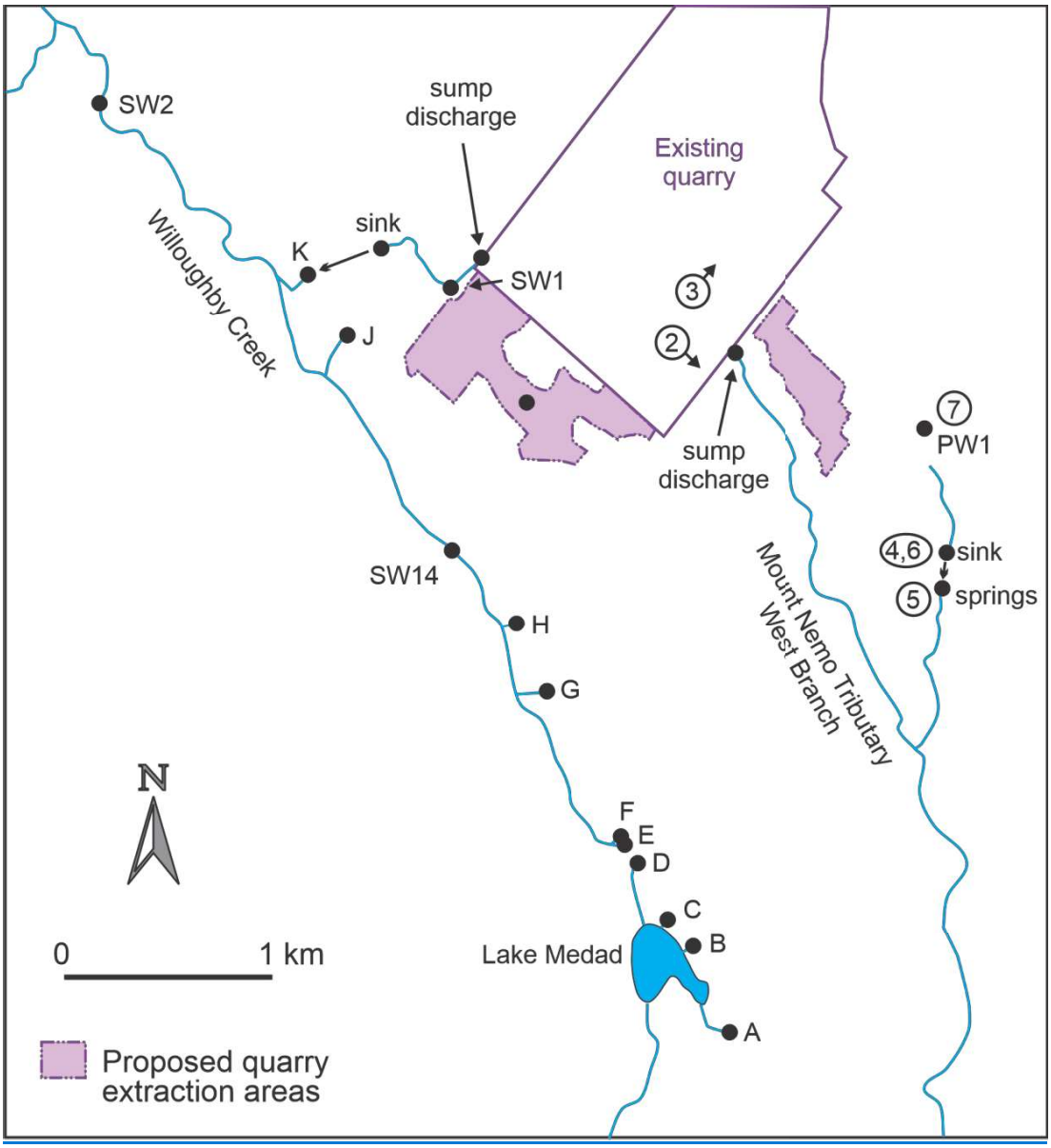

Figure 1a. Location of springs A to K, sinking streams near the quarry, and locations of the photos (circled numbers) shown in Figures 2 to 7.

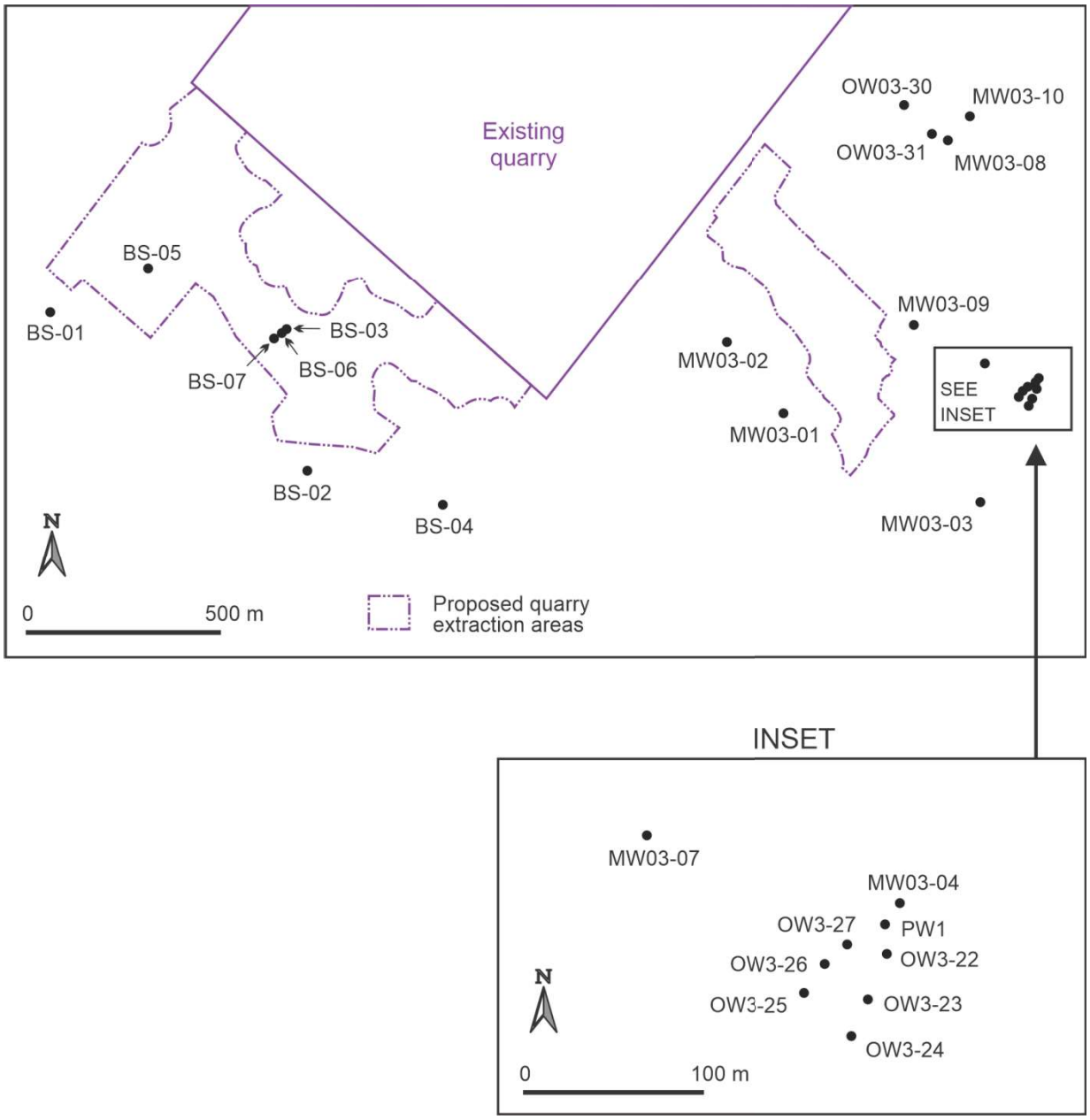

Figure 1b. Location of the wells referred to in this report.

Figure 2. Multiple ice deposits near the base of the quarry wall and spare ice higher in the wall below the processing plant. The location is shown in Figure 1.

Figure 3. A hydrologically-inactive large void near the base of the south-east face of the quarry, together with ice build-ups indicating much smaller channels that are active and discharge water.

Figure 4. Looking north towards the sinkpoint of the East Arm of the West Branch of Mount Nemo Tributary on March 14, 2005

Figure 5. Looking north towards the springs of the East Arm of the West Branch of Mount Nemo Tributary on March 14, 2005

Figure 6. Injection of uranine dye at the sinkpoint of the East Arm of the West Branch of Mount Nemo Tributary on March 22, 2005

Figure 7. Shallow closed depression close to the boundary of the extension lands on March 23, 2006.

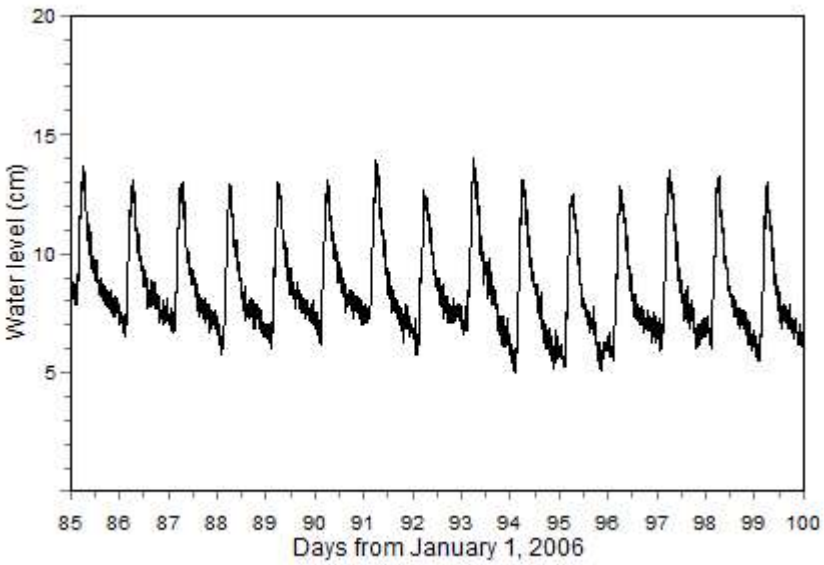

Figure 8. Water levels at Spring K from March 26, 2006 to April 9, 2006, showing a diurnal fluctuation due to pumping from the quarry sump to Willoughby Creek Tributary

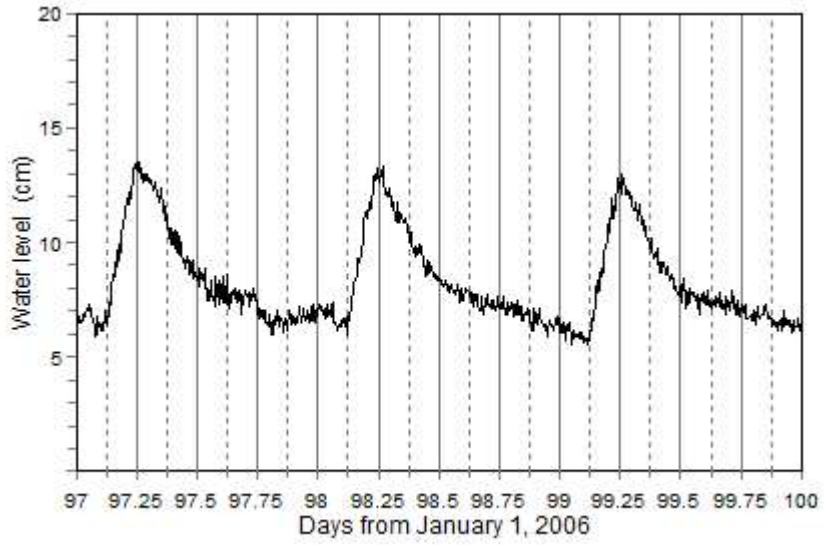

Figure 9. Water levels at Spring K for April 7, 8, and 9, showing a rise in water level at about 3 am and a peak at 6 am each day in response to pumping from the quarry sump.

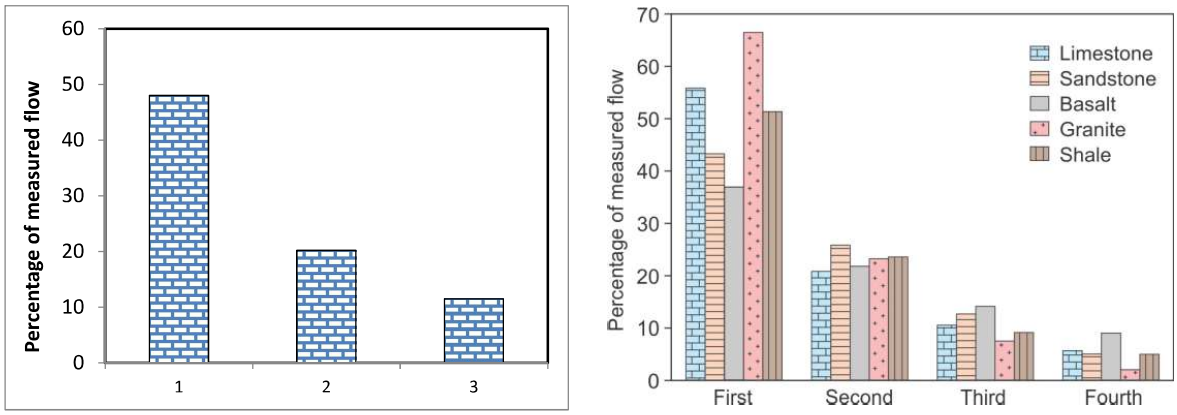

Figure 10. Average percentage of flow from the most produce fractures in the dolostone aquifer at Burlington (left) and in 77 wells in different bedrock lithologies (right). Data is from Table 7 (left) and from Worthington et al., 2016 (right).

16.7 Appendix A: Tracer testing

Tracer methodology for well to well tests

The tracers used were the fluorescent dyes uranine (also known as sodium fluorescein; Colour Index (CI) 45350), eosin (CI 45380) and phloxine B (CI 45410). Sodium fluorescein is the preferred dye since it is the most fluorescent and is the more detectable dye with both field and lab instruments; it was used in four of nine injections. All three dyes have very low toxicity and are approved for use in drugs in Canada (Food and Drugs Act, section C.01.040.2).

Grab samples were collected from the pumped discharge water and saved in 20 mL glass vials. Samples were collected at the end of the discharge line, which was located in a trailer 233 m from the pumping well. Samples were analyzed onsite in near real time on a Turner Designs Picofluor filter fluorometer. This instrument has two channels and can measure concentrations of two different dyes injected at the same time. The analysis on site gave approximate results that were ideal for planning subsequent tracer injections. After the completion of the tracer testing all samples were stored at 4o C and later reanalyzed on the filter fluorometer after being allowed to come to room temperature for 24 hours. Where three dyes were injected simultaneously, the filter fluorometer was only able to give approximate results, and selected samples were reanalyzed on a Photon Technology International scanning fluorometer in the laboratory of Dr. Chris Smart at the University of Western Ontario.

For each injection, the dye (previously diluted into four litres of water) was injected either by siphoning it down tubing to below the water table in each well or by pouring it directly into the monitor. In both cases a further 20 litres of the discharge water pumped from PW-1 was flushed down the tubing to ensure that all the dye was flushed from the container and tubing through the sand pack and into the bedrock. The amount of dye injected was calculated from two equations which give good predictions of tracer concentrations (Worthington and Smart, 2016). Small quantities of dye were used to ensure that there would be no offsite coloration of either surface water or groundwater.

The pumping test commenced at 15:50 on February 9th, 2006. The pumping rate was increased from 25 litres per minute to 32 litres per minute at 09:00 on February 10th to maintain a constant head in the well at a depth of 27.8 m below top of casing. Dye injections were made on February 10th, 11th and 12th. Sample collection followed a logarithmic schedule after dye injection, with the sampling interval increasing gradually from five minutes immediately after injection to one hour at 12 or more hours after injection. Sampling was terminated at the cessation of pumping at 12:40 on February 13th.

Tracer methodology for sink to spring tracer test

A tracer test was carried out on the West Arm of the East Tributary of Mount Nemo Tributary at the point where the stream sinks into the ground. Four springs were noted close to the edge of the pond where surface flow starts again. Conductivity and temperature measurements gave essentially identical readings from all four orifices. Samples were collected by hand from one of the eastern pair of springs and one of the western pair of springs. The springs were about 2 m apart and are 162 m from the injection point in an approximately southerly direction.

Tracing results at PW-1

On overview of the tracing results is shown in Figure A1 and Table A1 and A2. Three dyes were injected on February 10th into the deep bedrock monitors of the three wells closest to the pumping well, MW03-04A, OW03-22A and OW03-22A. Analysis of samples on the two-channel field fluorometer showed that at least two of the three dyes arrived quickly at the pumping well and peaked after a few hours. Slow recessions resulted in substantial concentrations after 24 hours in the pumped water, so larger amounts of dye were used in the injections on February 11th into the shallow bedrock

monitors of OW3-27B and OW3-22B. These arrived travelled quickly to the pumping well but had slow decreases in concentration, so the amount of tracer used was again increased for the final three traces on February 12th.

Only two dyes were injected on February 11th so the results from the filter fluorometer were used for the dye concentrations in Figure A4. Because of the triple dye injections on February 10th and February 12th, the scanning fluorometer was used to define the dye concentrations from these injections (Figures A2, A3, and A5). This analysis gave good results for all traces with the exception of Trace 3 and Trace 7. The peak concentration of Trace 3 was at 18:00 on February 10th, but the maximum concentration at that time is only shown by a higher minimum between the much larger urnaine and phloxine peaks at that time (Figure A3). There was no recovery for Trace 7 in the 24.3 hours until pumping stopped, so the travel time is longer than 24.3 hours.

Tracing results for sink to spring tracer test

Samples were analyzed in the field on a Turner Picofluor fluorometer, and sampling was stopped at 4.7 hours, by which time concentrations had returned to close to background. (Figure A6).

Interpretation of tracer test results for sink to spring tracer test

The sink to spring tracer test gives a groundwater velocity of 65 m/hour (Table A1 and Figure A6). This is close to the 73 m/hour geometric mean from a compilation of 3015 tracer tests (Worthington and Ford, 2009). The elapsed time to tracer arrival at the springs (Ta) was 1.9 hours and the elapsed time to peak concentration (Tp) was 2.5 hours. The Tp/Ta ratio is thus 1.3, which is typical for simple tracer tests in karst along a single conduit. The size of this conduit can be calculated from

$$A = Q / v$$

where A is the cross-section of the conduit, Q is conduit discharge, and v is conduit velocity. A discharge of 6 L/s was measured upstream of the sink, and the calculated conduit cross-section is 0.33 m^2. A discharge of 5.3 L/s was calculated from the dye recovery data, assuming 100% recovery. This latter discharge gives a conduit cross-section of 0.29 m^2.

There are several sinkpoints spread over a distance of several metres. Similarly, at the pond there are several springs spread over several metres. Consequently, the cross-section area of 0.3 m^2 is divided between several conduits at the upstream and downstream end of the flow path. In between there could be a single conduit or multiple conduits that add up to 0.3 m^2. The water table is less than one metre below the surface along most of the flow path and so conduit development in the shallow weathered or epikarst zone is likely. This would favour there being multiple conduits.

The creek discharge downstream of the pond was gauged at 8 L/s, the temperature of the water was 4.2 ^oC and the conductivity was 463 µS/cm. This compares with 1.9 ^oC and 369 µS/cm in the creek upstream of the sink and 2.3 ^oC and 497 µS/cm at the springs that were sampled for dye. These data show that the 2 L/s increase in discharge from the sinkpoint to the pond outlet is accounted for by groundwater with a conductivity of 745 µS/cm. This value is similar to the conductivity measured in bedrock and overburden wells in the proposed extension area (Golder Associates, 2004).

The tracer test does not provide direct information on the depth of the conduit linking the sink to the spring. However, caves in similar environments, such as Nexus Cave in Hamilton follow a generally sub-horizontal pathway in the top few metres of the bedrock (Buck et al., 2002). The conduit here is similarly likely to be found in the top few metres of the bedrock.

Interpretation of tracer test results from well to well tests

The groundwater velocities measured for the well to well tests were all at least an order of magnitude slower than the sink to spring test (Table A2). Furthermore, the dispersion of dye is much greater, with the ratio Tp/Ta ranging from 2.2 to 6.9, which is much higher than the ratio of 1.3 for the sink to spring test. The higher dispersion shows that the flow paths between the injection wells and pumping well cannot be thought of as single fractures or channels. Instead, the traces suggest that there are multiple pathways that the dye followed and that the apertures of these pathways vary substantially. Such multiple pathways are especially clear in traces #1 and #8, which both have two tracer peaks.

The tracing results can be used to calculate a range of fracture or channel apertures, and two methods are used here. Both methods use the simplifying assumption that the pathways are circular channels or pipes. Maximum groundwater gradients can be calculated from the horizontal distance and the difference in head between the tracer injections wells and PW-1. However, the actual groundwater gradients may be less because some of the inflow to the well cascades down the well from further up the well. Following the end of the pumping test on February 13th, 2006, water could be heard cascading into the well until the water level rose to a depth of 6.01 m. The sound of the cascading water gradually diminished over time, indicating that there was inflow from several bedding planes. The gradient from the injection well to -6.01 m in the pumping well represents the minimum hydraulic gradient. Channel diameter can be calculated using the Hagen-Poiseuille equation for laminar flow in a pipe. Results for an assumed groundwater temperature of 10 ^{o}C range from <0.03 mm to 0.27 mm (Table A3). The Hagen-Poiseuille equation assumes flow in a smooth pipe. Channels in the bedrock are not smooth and so actual apertures will be somewhat larger than these calculations indicate.

The second method of calculating utilizes the known pumped discharge from PW-1 (32 L/min). It is assumed that the well intersects a number of circular channels and that water flows from both channel openings into the well in each case. The Darcy-Weisbach equation is used, which assumes turbulent flow, with a friction factor of, which is an average value for karst conduits. The range of hydraulic gradients of 0.18 to 0.86 is the same as in Table A3, and calculations are given for 2, 5, and 10 channels. The results are given in Table A4. The calculated Reynolds Numbers of at least 2100 confirm that flow is turbulent, and the channel diameter ranges from 9 mm to 24 mm.

The results from Tables A3 and A4 bracket the likely range of channel apertures in the aquifer. There are likely to be many channels with diameters in the range 0.1-1 mm, a smaller number in the range 1-10 mm, and relatively few with diameters > 1cm.

References

Buck, M.J., Worthington, S.R.H., and Ford, D.C., 2003. Earth science inventory and evaluation of the Eramosa Karst Area of Natural and Scientific Interest. Ontario Ministry of Natural Resources, Guelph, 51 p.

Golder Associates, 2004, Hydrogeological and water resources assessment of the proposed Nelson Quarry Co. Extension.

Worthington, S.R.H., and D.C. Ford, 2009, Self-organized permeability in carbonate aquifers. Ground Water, 47, no. 3, 326-336.

Worthington, S.R.H., and Smart, C.C., 2016. Determination of tracer mass for effective groundwater tracer tests. Carbonates and Evaporites, 31, 349-356.

Table A1 Tracer Injection details

Test number	Tracer Injection Date	Time	Dye	Mass of dye (g)	Injection location
1	Feb. 10	11:14	Uranine	1.96	MW03-04A
2	Feb. 10	12:26	Phloxine	1.42	OW03-22A
3	Feb. 10	13:04	Eosine	1.58	OW03-27A
4	Feb. 11	11:29	Phloxine	17.83	OW03-27B
5	Feb. 11	11:34	Uranine	6.10	OW03-22B
6	Feb. 12	09:56	Eosine	98.57	OW03-27B
7	Feb. 12	11:09	Uranine	6.25	MW03-04B
8	Feb. 12	11:20	Phloxine	61.24	OW03-27A
9	March 22	11:18	uranine	0.48	Sinking stream

Table A2 Tracer recovery details

Test #	Recovery location	Distance from injection location (m)	Travel time to tracer arrival (Ta – hours)	Travel time to tracer peak (Tp – hours)	Dye recovery (%)	Tp/Ta	Velocity (m/d)
1	PW-1	13.7	0.77	2.1	7.5	2.7	160
2	PW-1	16.1	1.2	5.4	32	4.5	72
3	PW-1	23.7	(2.2)	(4.8)	N.C.*	(2.2)	120
4	PW-1	23.7	1.4	4.5	35	3.8	130
5	PW-1	16.1	0.52	3.6	33	6.9	110
6	PW-1	23.7	1.3	4.4	19	3.4	130
7	PW-1	13.7	>24.3	>24.3	0	-	<13
8	PW-1	23.7	<3	4.7	9.2	-	120
9	Pond spring (west)	162	1.9	2.5	~100	1.3	1600
9	Pond spring (east)	162	1.9	2.5	~100	1.3	1600

* Notes:
N.C. = not calculated

Table A3 Calculated channel apertures from tracer tests

Well	Trace #	Tracer velocity (m/d)	Distance to PW-1	Difference in head (m)	Channel diameter (mm)
MW03-04A	1	160	13.7	23	0.095
MW03-04B	7	<13	13.7	4.3	<0.046
MW03-04B	7	<13	13.7	23	<0.028
OW03-22A	2	72	16.1	23	0.066
OW03-22B	5	110	16.1	4.3	0.27
OW03-22B	5	110	16.1	23	0.15
OW03-27A	3	120	23.7	23	0.091
OW03-27A	8	120	23.7	23	0.093
OW03-27B	4	130	23.7	4.3	0.19
OW03-27B	4	130	23.7	23	0.095
OW03-27B	6	130	23.7	4.3	0.19
OW03-27B	6	130	23.7	23	0.096

Table A4 Calculated channel apertures from inflow to PW-1

Number of channels	Discharge per channel (mL/s)	Hydraulic gradient	Channel velocity (m/s)	Channel diameter (mm)	Reynolds Number
10	53	0.18	0.24	13	2100
10	53	0.86	0.45	9	2800
5	107	0.18	0.28	17	3100
5	107	0.86	0.52	12	4200
2	267	0.18	0.34	24	5400
2	267	0.86	0.63	18	7400

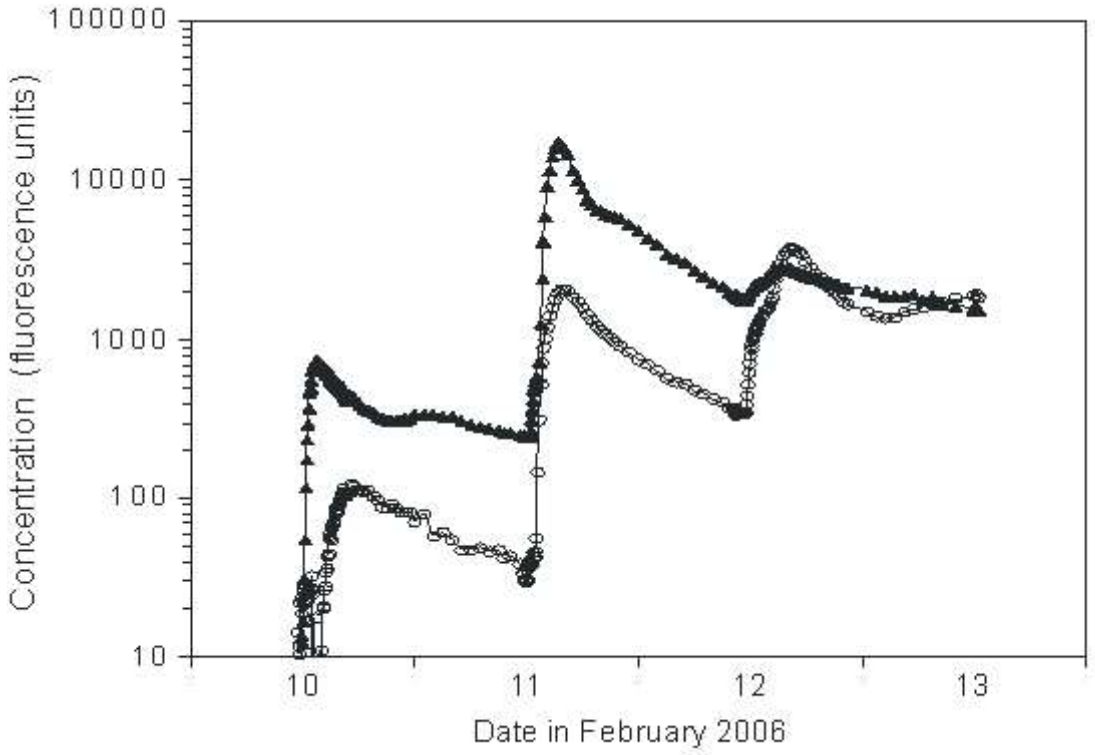

Figure A1 Dye concentrations at PW-1 on February 10-13, 2006 on the green channel (triangles) and red channel (circles) of a Turner Picofluor field fluorometer

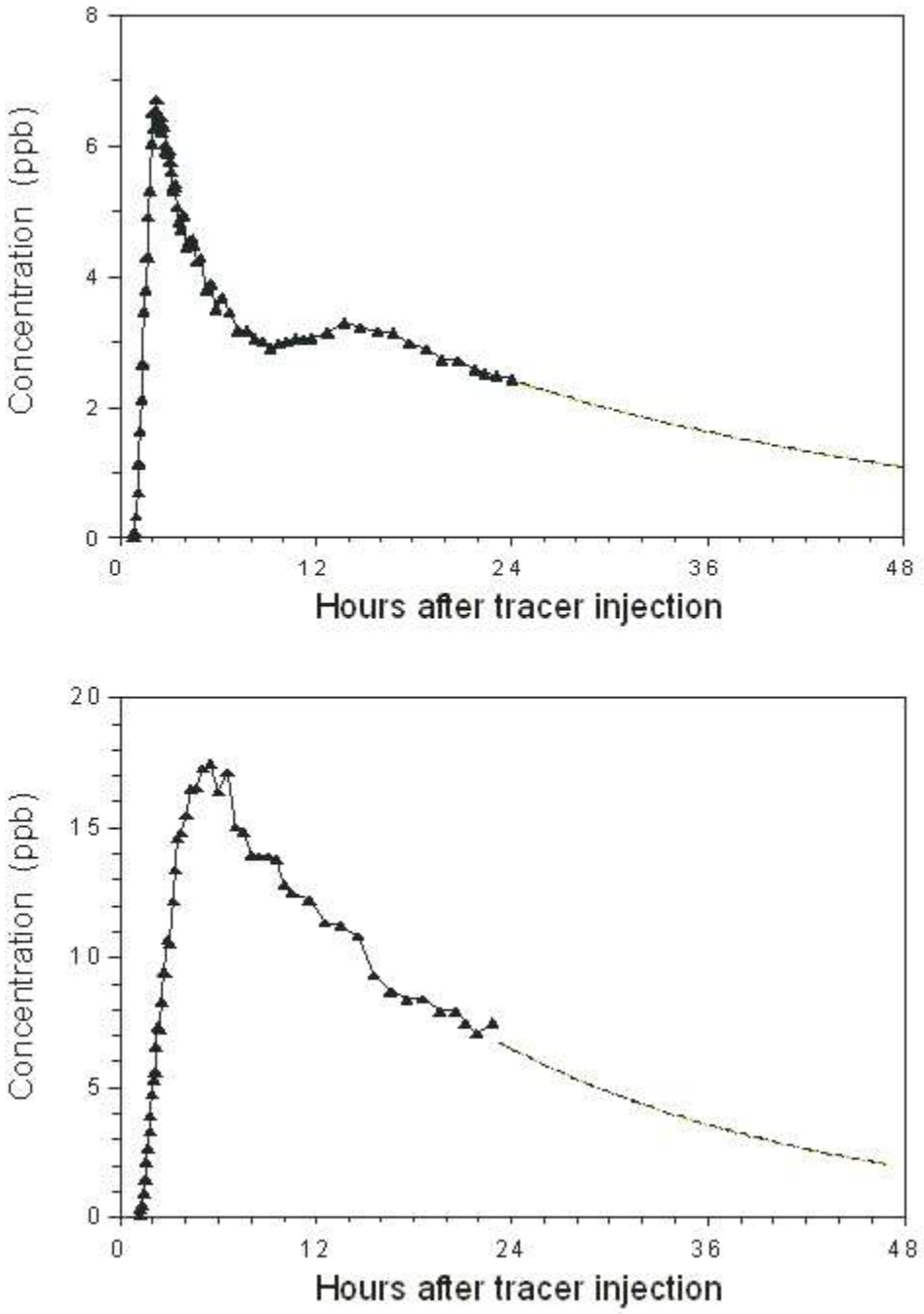

Figure A2 Dye concentrations at PW-1 for Trace 1 (uranine, top) and Trace 2 (phloxine, bottom), showing calculated exponential recessions

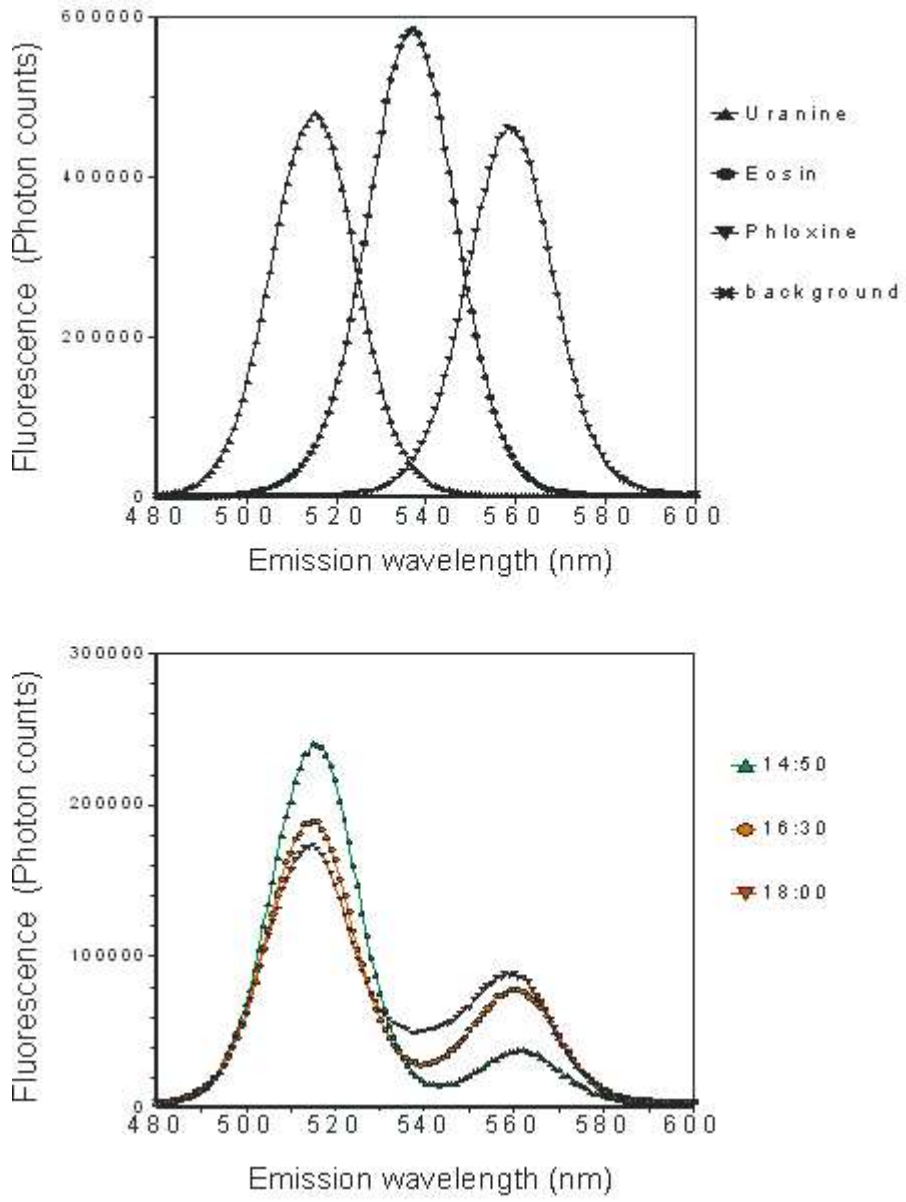

Figure A3 Fluoroscence spectra for standards of 10 µg/L uranine, 100 µg/L eosin and 100 µg/L phloxine (top) and for three samples from PW-1, showing decreasing concentrations of uranine and increasing concentrations of eosin and phloxine between 14:50 and 18:00 on February 10, 2006.

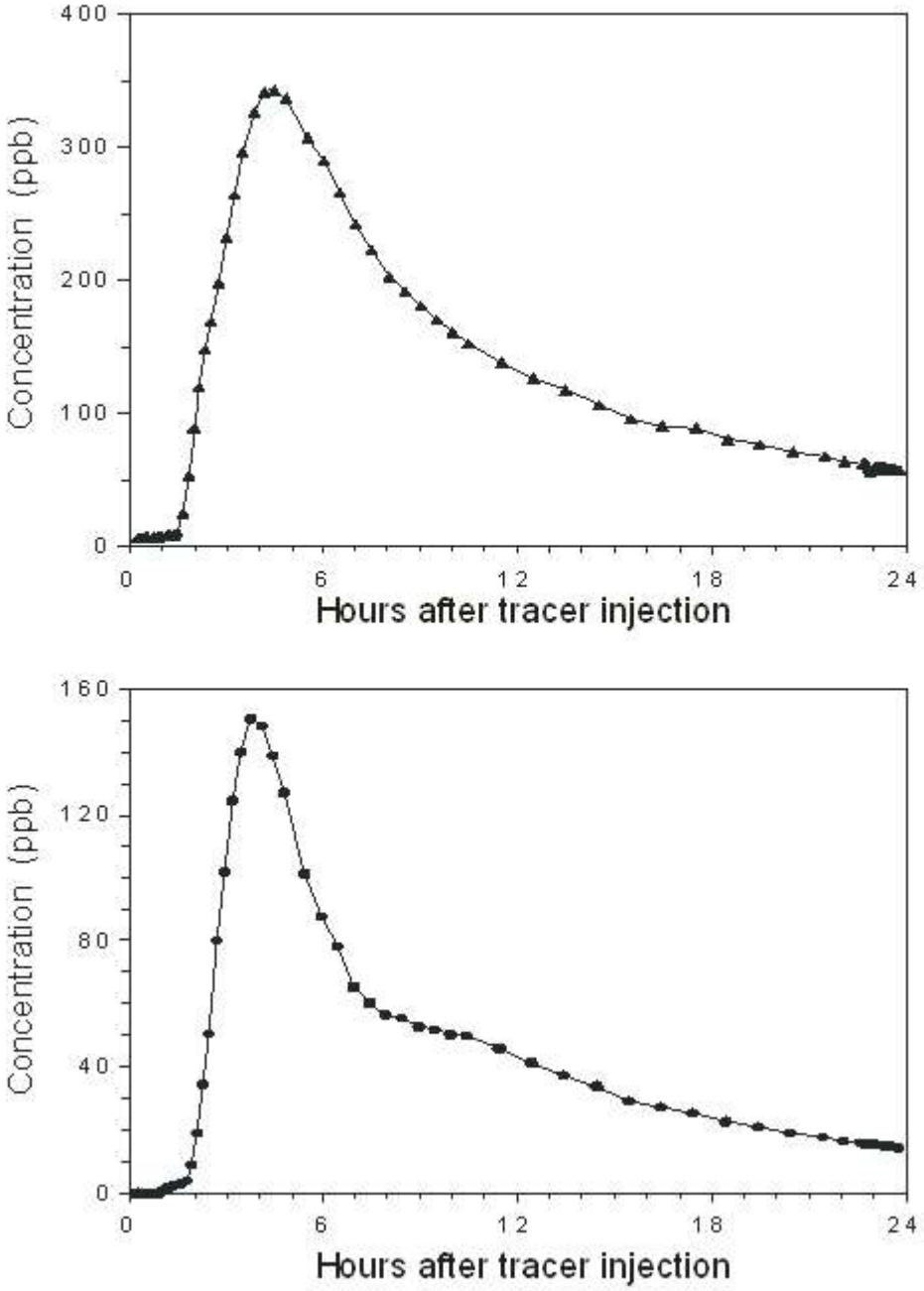

Figure A4 Dye concentrations at PW-1 for Trace 4 (phloxine, top) and Trace 5 (uranine, bottom).

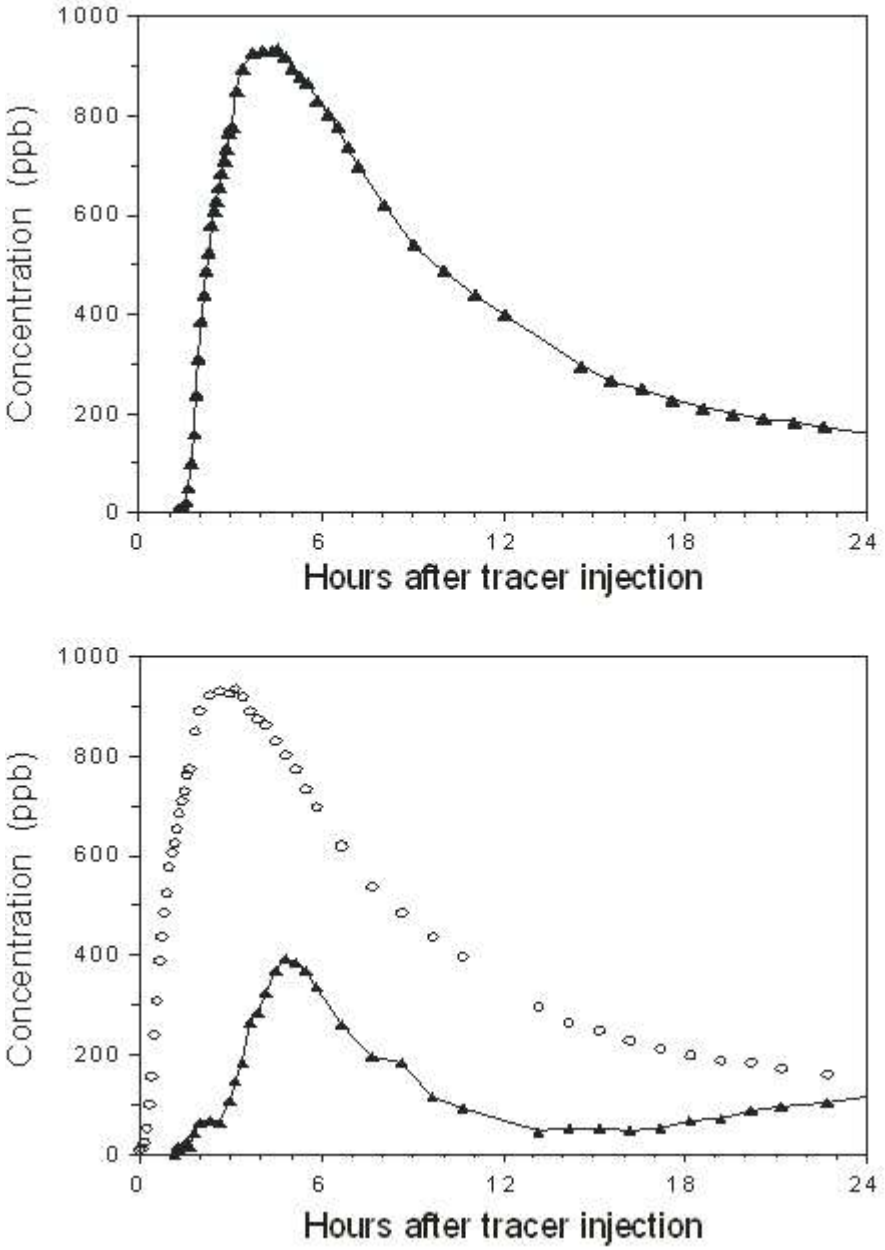

Figure A5 Dye concentrations at PW-1 for Trace 6 (eosin, top) and Trace 8 (phloxine, bottom). In the lower figure, the concentrations of eosin are shown for comparison.

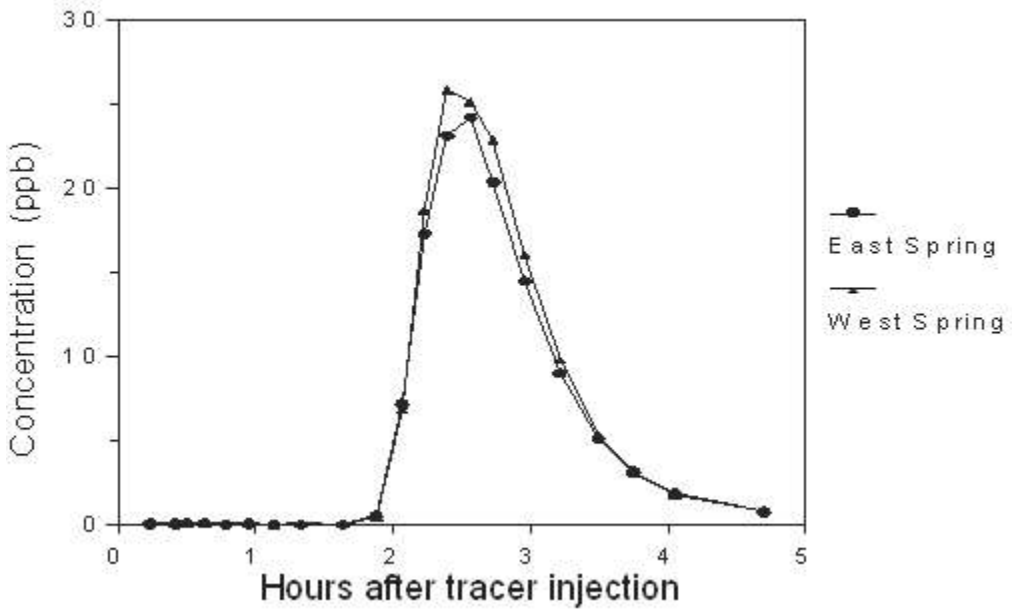

Figure A6 Concentrations of uranine for Trace 9 on March 22, 2006 at two springs in the pond on the East Arm of the West Branch of Mount Nemo Tributary.

Appendix B. Select video, televiewer, and flowmeter logging

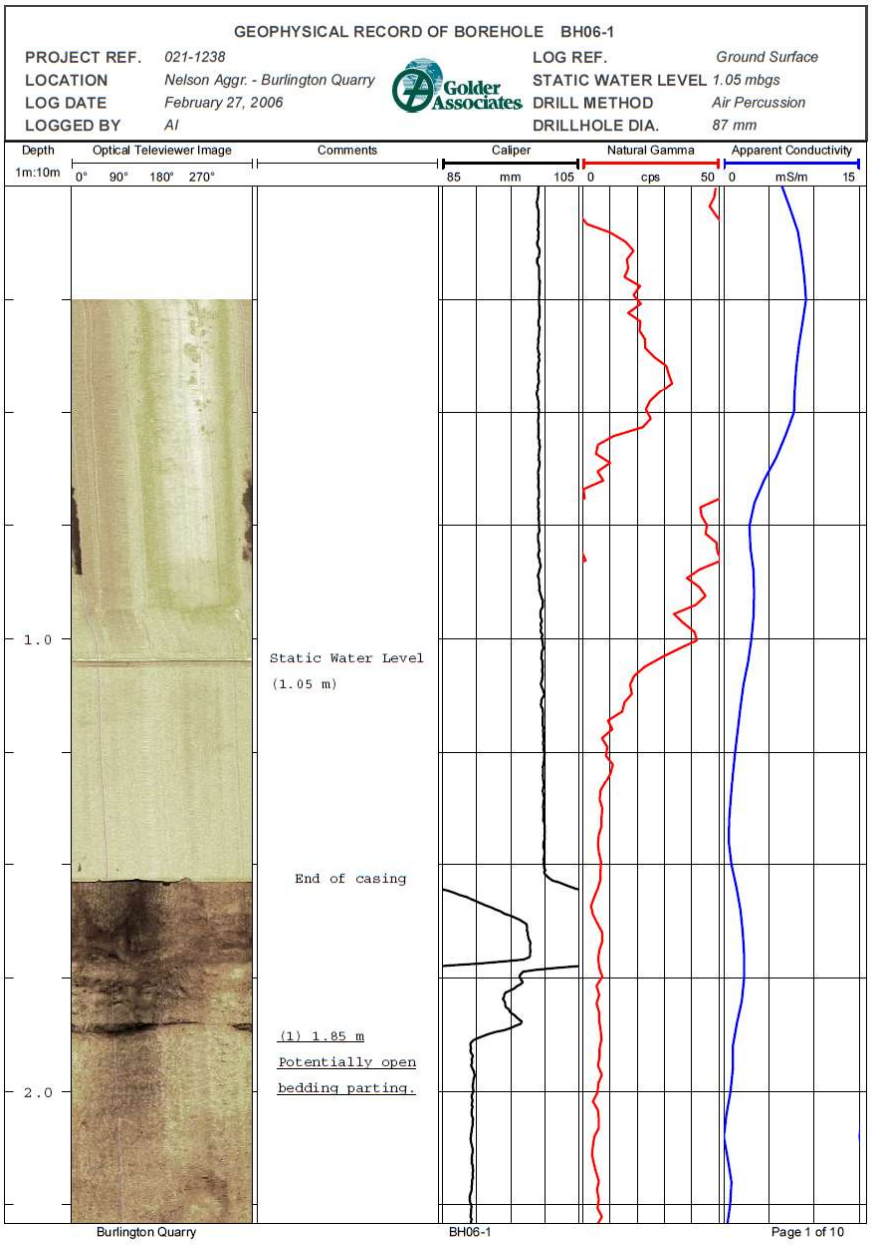

Figure A7. Optical televiewer and other geophysics logs from Well BH06-1

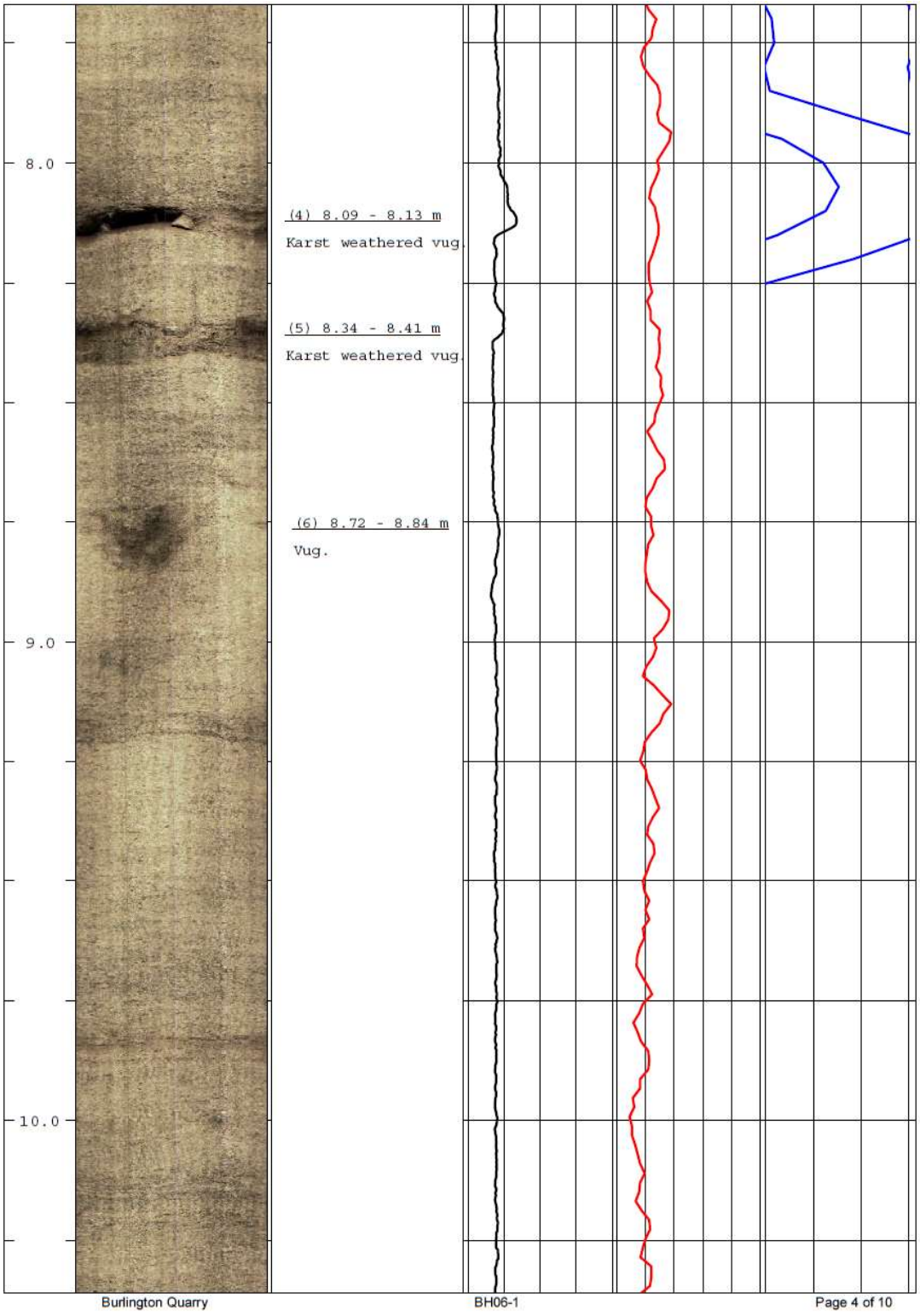

Figure A7. (continued) Optical televiewer and other geophysics logs from Well BH06-1

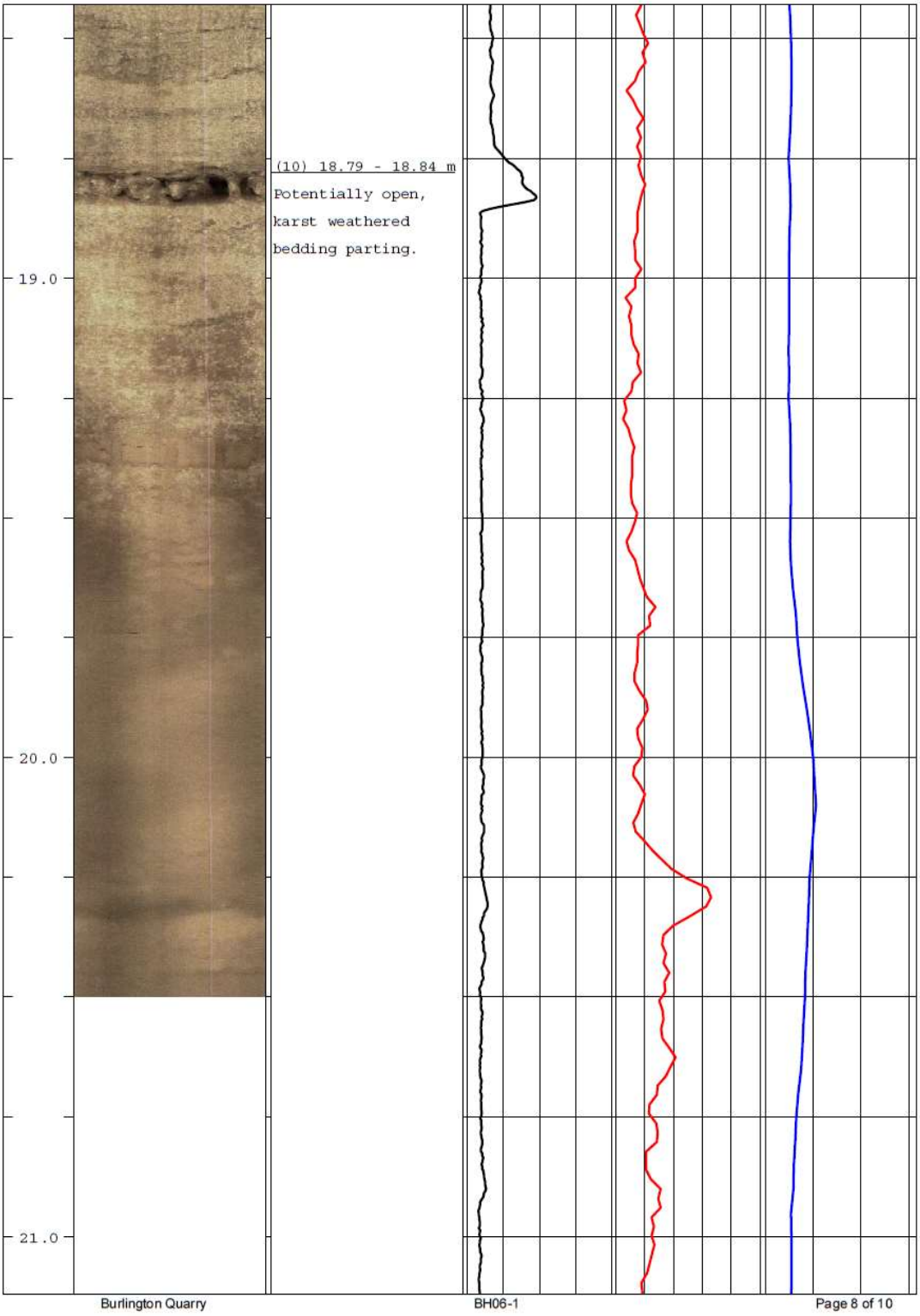

Figure A7. (continued) Optical televiewer and other geophysics logs from Well BH06-1

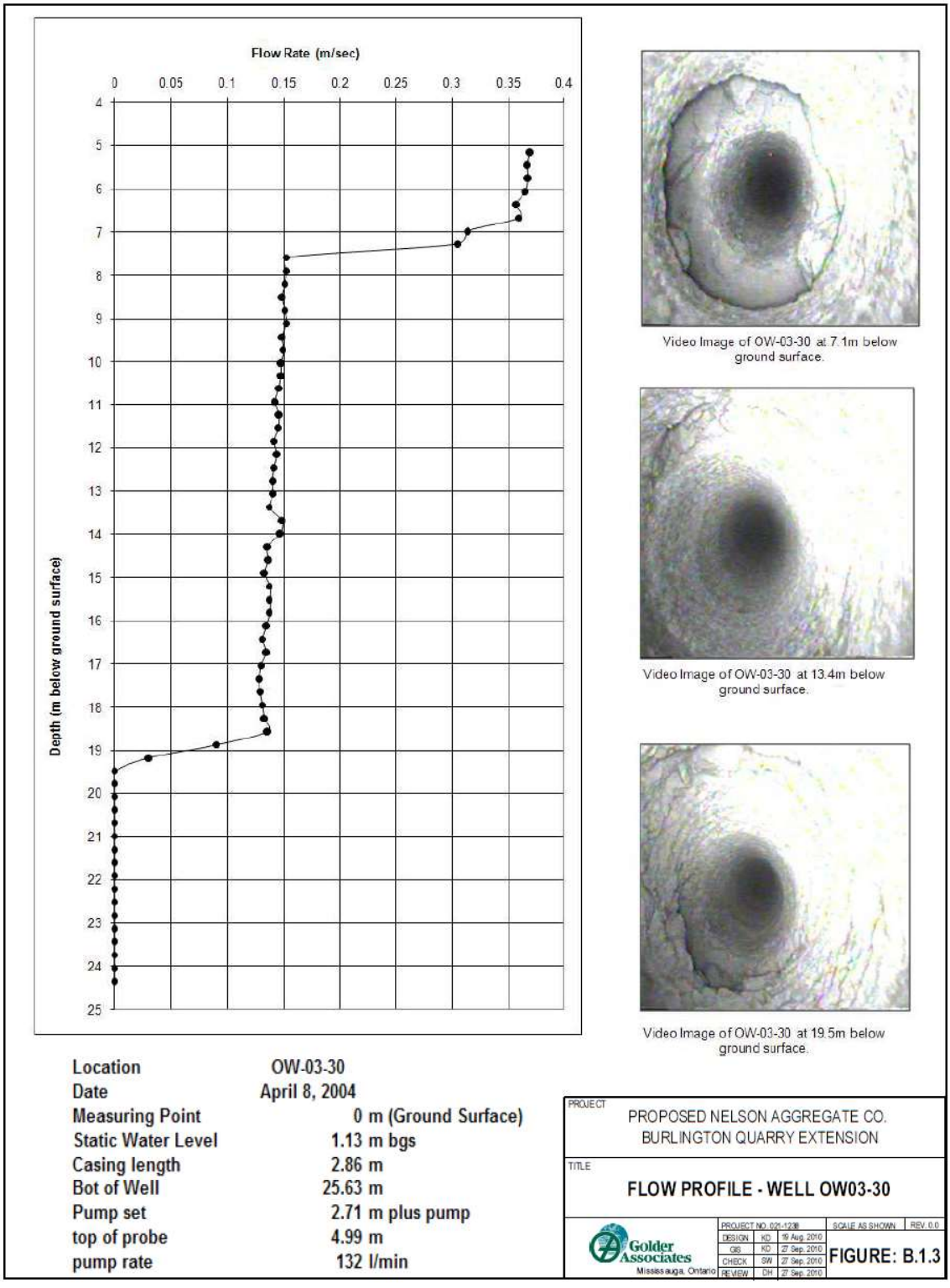

Figure A8. Flowmeter and video images in Well OW3-30

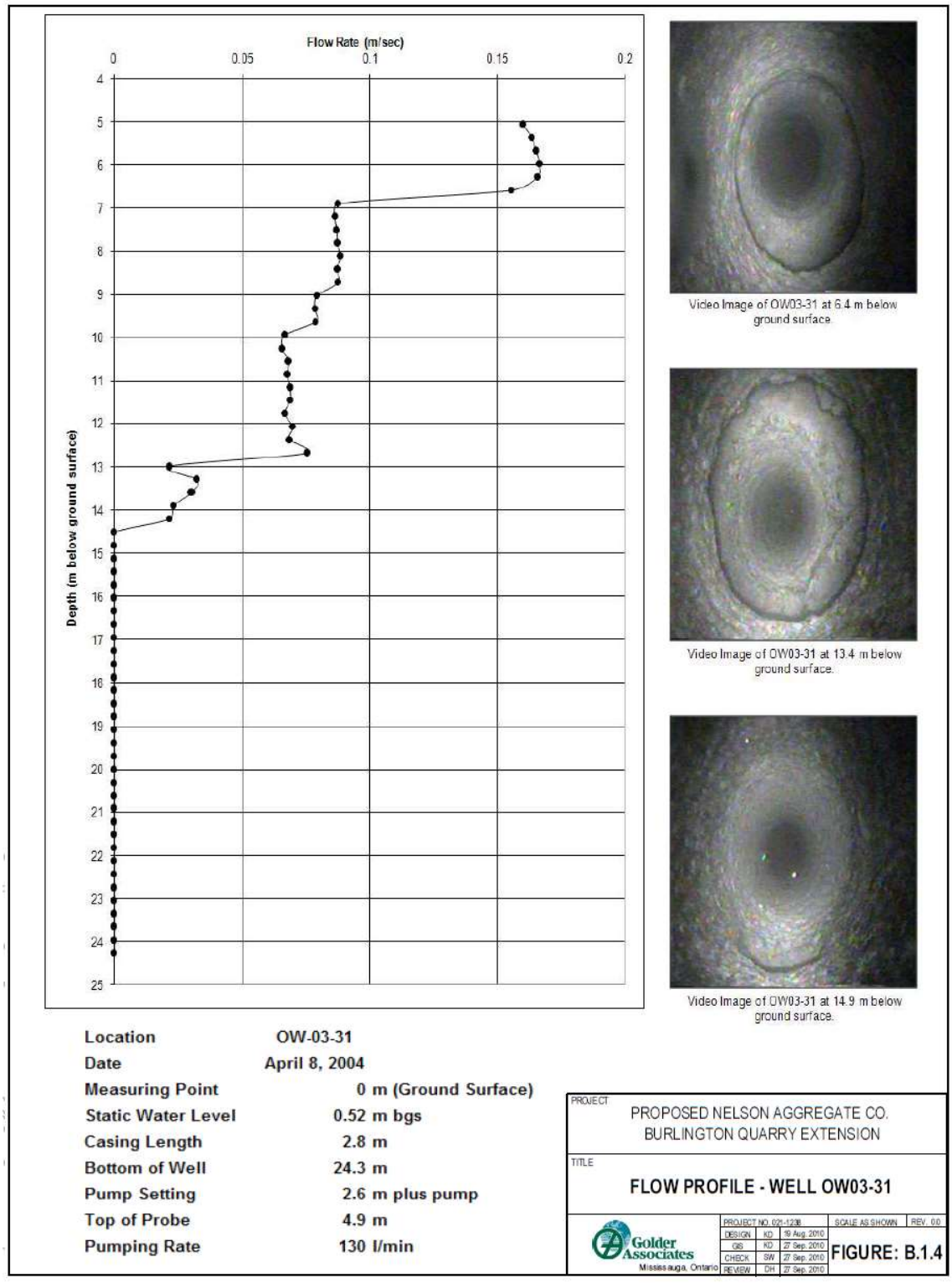

Figure A9. Flowmeter and video images in Well OW3-31

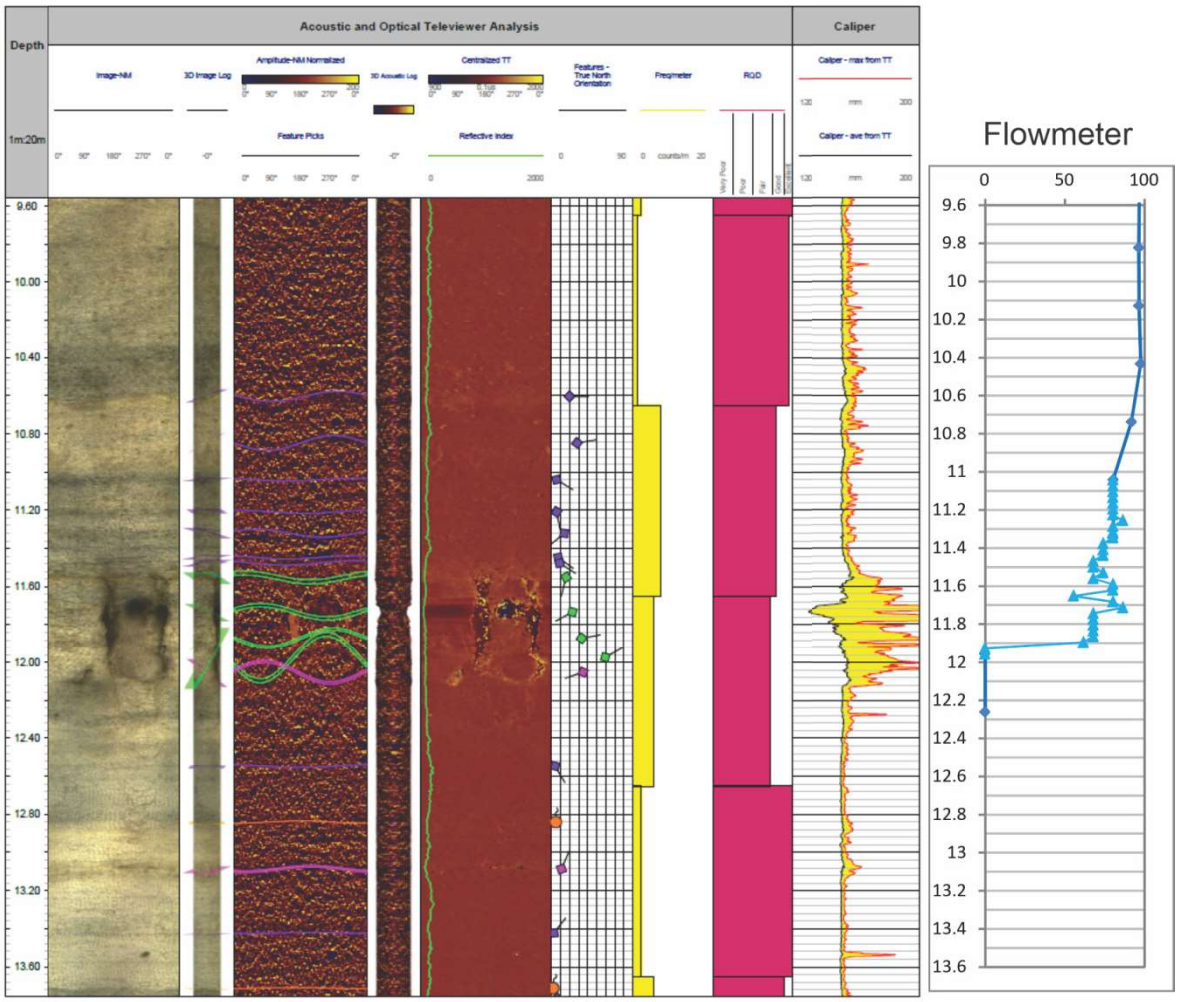

Figure A10. Geophysics logs of Well BS-05

Appendix C. Electrical conductivity and temperature profiles from wells

Electrical conductivity (EC) and temperature profiling was carried out in wells BS-06 and BS-07 using a Heron Instruments Inc. conductivity and temperature meter. The probe was lowered into the well and measurement recorded at 0.5 m intervals. More frequent measurements were made where there were substantial changes in conductivity.

BS-06 was profiled before, during, and after the 72 hour pumping test at BS-06, which is 37 m from BS-07 (Figures A11 and A12). Results show that EC is substantially higher at the bottom of the well, with the greatest change in EC occurring at a depth of 21.0 m to 21.2 m. There is no change in temperature at this depth, but there substantial changes between 8 m and 8.5 m and between 16 m and 19 m. Flow either up or down the well is indicated where there is little change in values with depth, such as between 9 m and 16 m for both EC and temperature. The substantial change in temperature below 16 m suggests that most flow down the well is exiting via a fracture at 16 m. The lowest EC two hours after cessation of pumping, during the recovery phase, suggests that there was ingress of low EC water from a fracture at 9 m depth and that flow was down the well, with most flow exiting the well via at fracture at 21.1 m. Changes in EC at the very bottom of the well suggest that there are one or more active fractures at this depth.

BS-07, the pumping well, was profiled before and after pumping. The EC profile before pumping shows that there was a substantial increase in EC at a depth of 24 - 25 m. A temperature profile was not taken before pumping. The first profile after the end of the pumping test was taken two hours after the cessation of pumping, and immediately after the removal of the submersible pump. There was a rapid increase thereafter in the bottom metre of the well, from 600 µS/cm at 2 hours, to 690 µS/cm at 2.2 hours, to 810 µS/cm at 2.5 hours. This rapid change suggests that the submersible pump, which was close to the bottom of the well and occupied much of its cross-section, was restricting upward flow. There are also changes in EC and temperature at 10.5 to 11 m, and 19 to 21.5 m.

Overall, the changes in EC and temperature with depth and over time suggest that there are one or more open fractures in well BS-07 between 8 m and 9 m, between 16 m and 18 m, and at 21.1 m. In well BS-06, there are major open fractures at 10.8 m and 25.1 m, with probably three less important fractures between 18.5 m and 21.5 m. Furthermore, the changes in EC and temperature suggest that the open fractures must persist laterally and be well-connected, resulting in contrasting values at different depths and rapid changes in values over time.

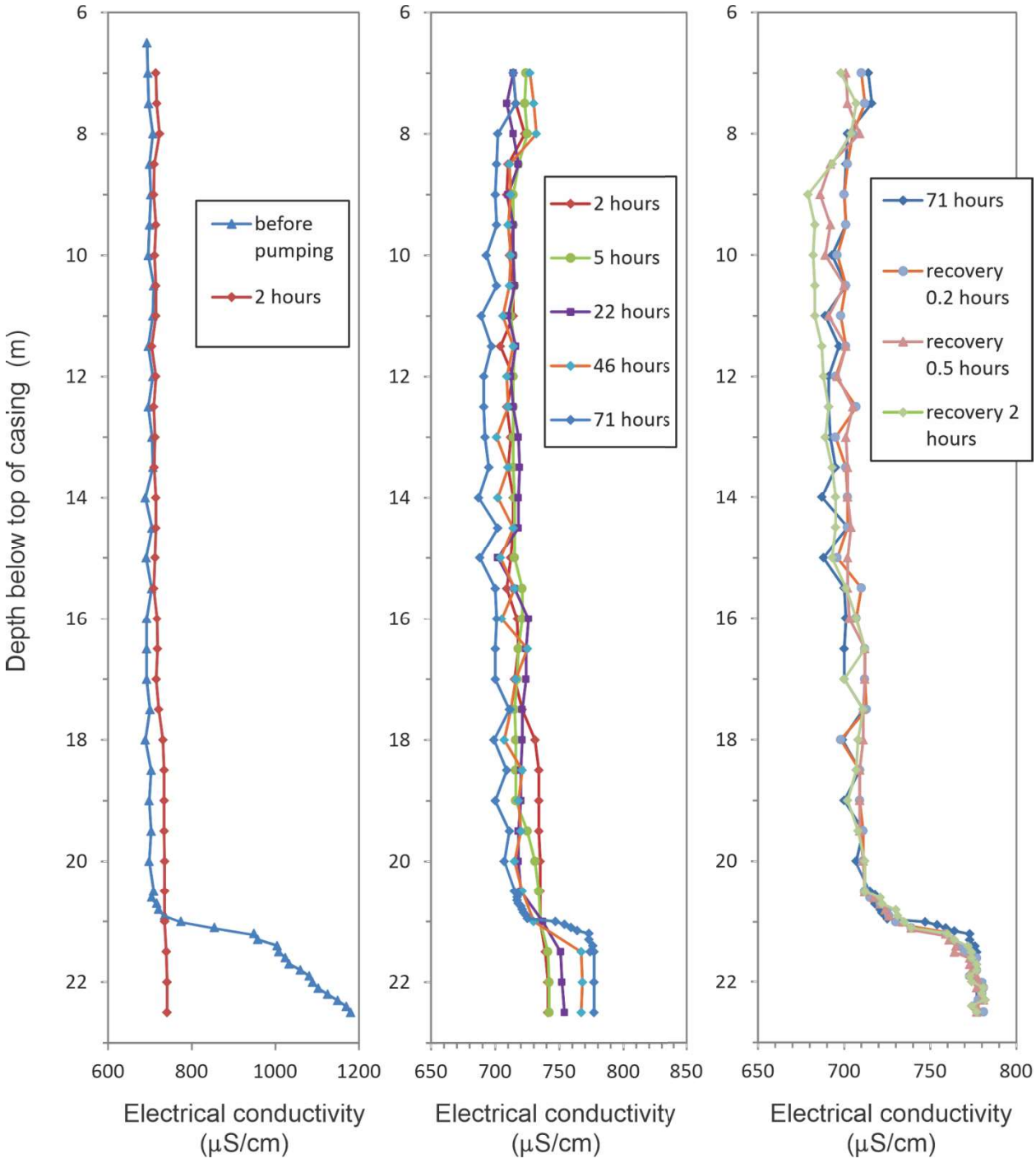

Figure A11. Electrical conductivity profiles at Well BS-07 before, during and after the pumping test at BS-06.

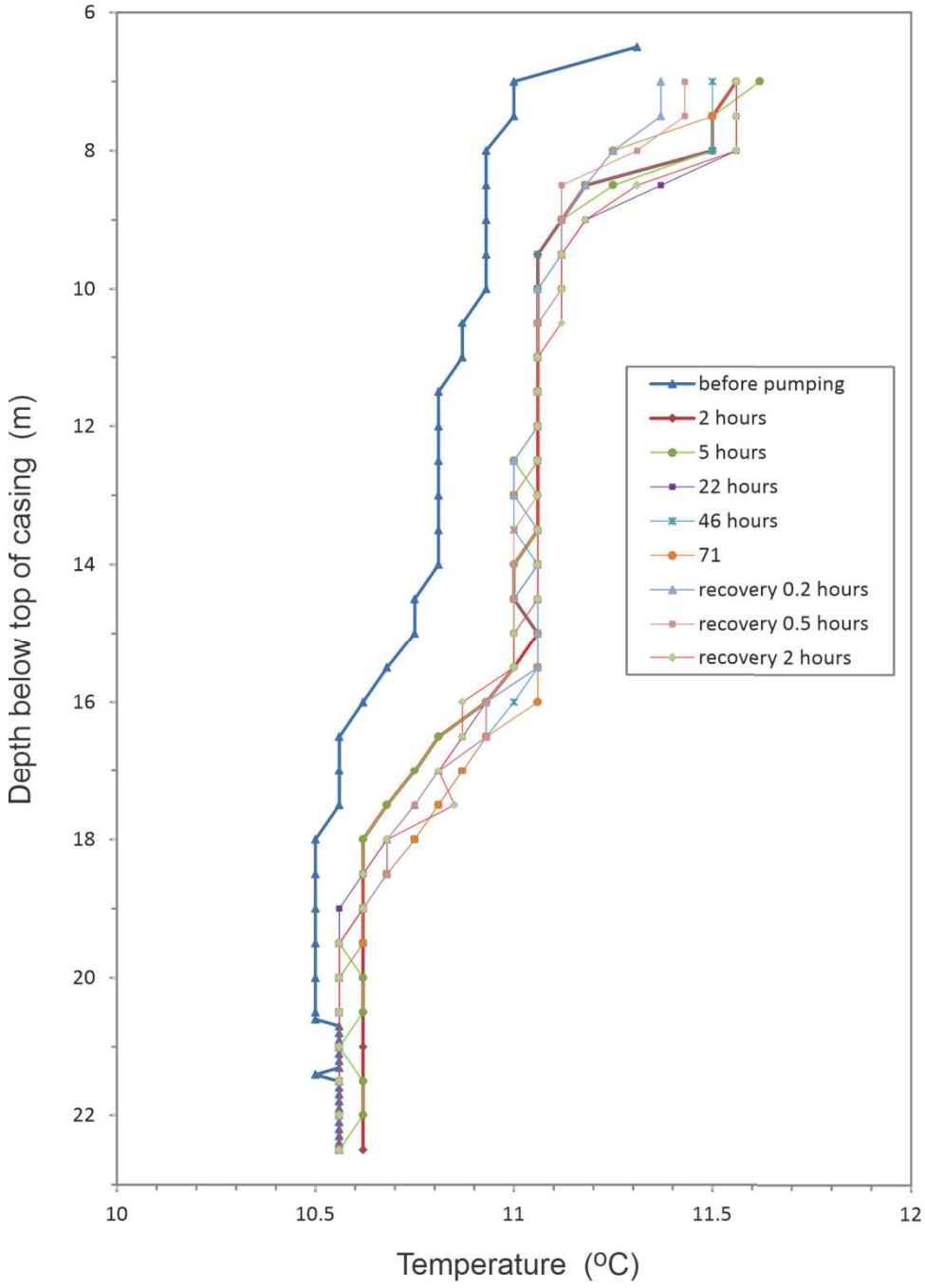

Figure A12. Temperature profiles at Well BS-07 before, during and after the pumping test at BS-06.

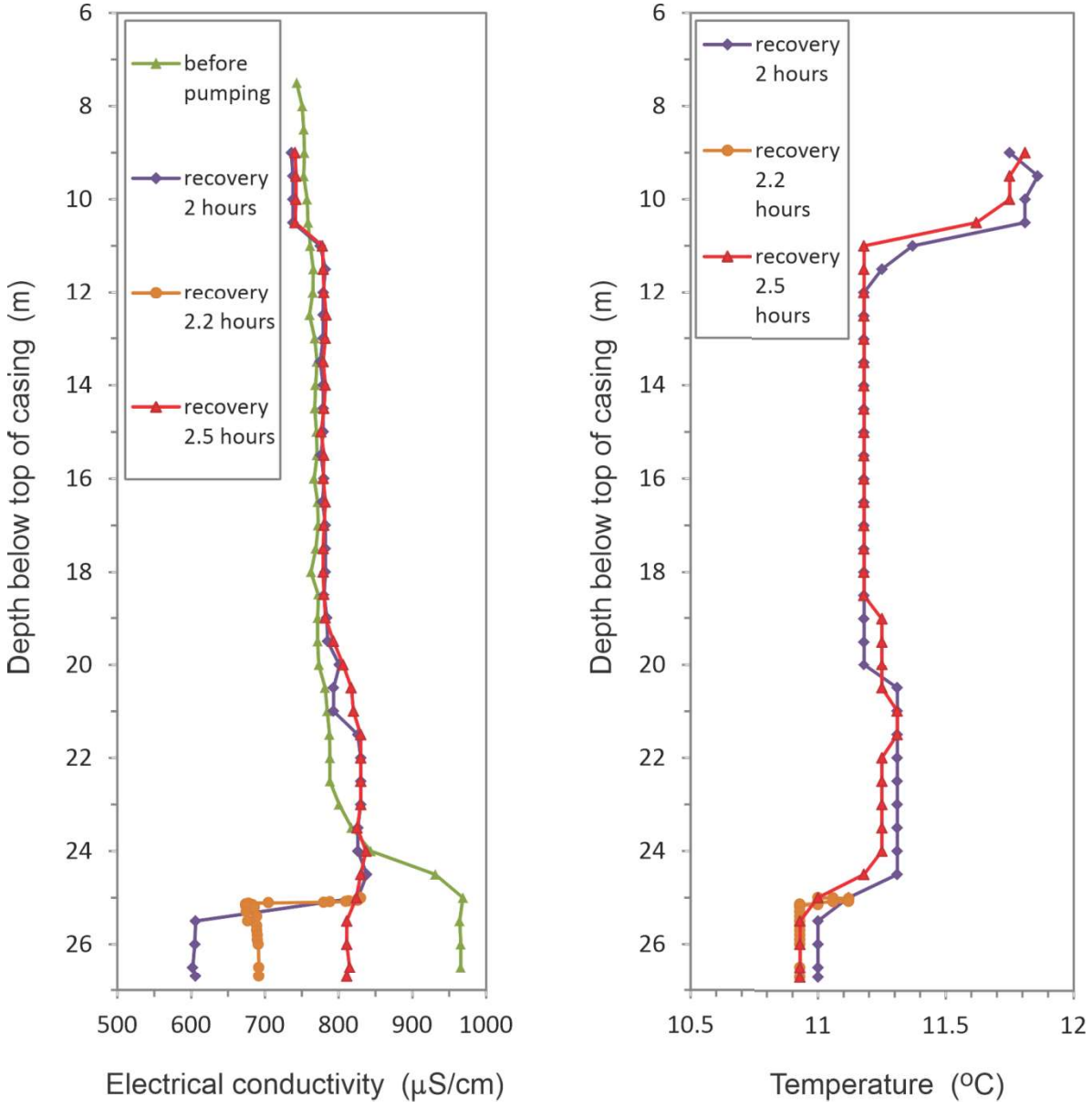

Figure A13. Electrical conductivity and temperature profiles at Well BS-06 before and after the pumping test at BS-06.